Isotopic equilibrium between raindrops and water vapor during the onset and the termination of the 2005-2006 wet season in the Bolivian Andes

Françoise Vimeux, Camille Risi

Isotopic equilibrium between raindrops and water vapor during the onset and the termination of the 2005-2006 wet season in the Bolivian Andes

Françoise Vimeux[1,2] and Camille Risi[3]

1- HydroSciences Montpellier (HSM), UMR 5569 (UM, CNRS, IRD), 34095 Montpellier, France.

2- Institut Pierre Simon Laplace (IPSL), Laboratoire des Sciences du Climat et de l'Environnement (LSCE), UMR 8212 (CEA, CNRS, UVSQ), 91191 Gif-sur-Yvette, France.

3- Institut Pierre Simon Laplace (IPSL), Laboratoire de Météorologie Dynamique (LMD), UMR 8539 (CNRS, ENS, X, UPMC), 75252 Paris, France

Corresponding author

Françoise Vimeux, HydroSciences Montpellier (UM, CNRS, IRD) and Laboratoire des Sciences de Climat et de l'Environnement (CEA, CNRS, UVSQ), CEA Saclay, Orme des Merisiers, Bât. 714, 91191 Gif-sur-Yvette, France, Francoise.Vimeux@lsce.ipsl.fr

Abstract

The isotopic equilibrium state between precipitation and low-level water vapor is a common assumption in numerous paleoclimate and atmospheric studies based on water stable isotopes. However, the paucity of field observations limits the validation of this assumption. This study examines the isotopic equilibrium state from event-based precipitation and daily near-surface water vapor samples collected during the onset and the termination of the 2005-2006 wet season in the Bolivian Andes (Zongo valley, 16°09'S, 68°07'W). Our observations show that the observed isotopic composition of precipitation (δD_p) deviates from the theoretical isotopic composition of precipitation at equilibrium with water vapor (δD_{p_eq}). Disequilibriums ($\Delta D_{p\_eq} = \delta D_p - \delta D_{p\_eq}$) are mostly negative (73%), indicating that precipitation is more depleted than a condensate that would have been formed from surface water vapor, and half of them are between -10 and +10‰. They are significantly correlated to δD_p (r^2=0.30, n=70, p<0.001) suggesting that controls on δD_p also impact ΔD_{p_eq}. Although equilibrium state does not prevail at the individual rain event scale, a strong relationship is observed between δD_p and δD_{p_eq} over the whole period of field samplings (r^2=0.86, n=70, p<0.001). The review of possible causes to explain the disequilibriums shows that below-cloud rain evaporation and diffusive exchanges are little involved. Other local processes such as rain type, condensation conditions and surface water recycling appear as better candidates to explain ΔD_{p_eq}. Lastly, we explore how local processes affect δD_p. We show that large-scale dynamic along air masses history is dominant (nearly 80%) to explain δD_p whereas local effects are dominant to explain deuterium excess in precipitation. In consequence, we conclude that δD_p is a correct candidate to examine and to reconstruct large-scale atmospheric processes from past to present time scales.

Keywords:

Water stable isotopes, isotopic equilibrium, below-cloud processes, Bolivia, Andes.

1-Introduction

Stable isotopes of precipitation and water vapor are increasingly cited as a useful tool to explore a range of atmospheric processes (Galewsky et al., 2016 for a recent review). Stable isotopes of precipitation are also widely recognized to reconstruct past environment and climate. Usually, the isotopic composition of water is defined as follows in per mill (‰):

$$\delta^{18}\mathrm{O} \text{ or } \delta\mathrm{D}\ (‰) = \left(\frac{\mathrm{R_{sample}}}{\mathrm{R_{SMOW}}} - 1\right) \cdot 1000 \quad (1)$$

Where R is the isotopic ratio between heavy ($H_2{}^{18}O$ for $\delta^{18}O$ and $HD^{16}O$ for δD) and light ($H_2{}^{16}O$) molecules in rain or water vapor and SMOW (Standard Mean Ocean Water) is the international standard for water isotopic measurements (i.e, $\delta_{SMOW} = 0‰$ by definition).

In clouds, the formation of droplets by condensation of ambient water vapor follows the thermodynamic law that leads the two phases towards isotopic equilibrium. This isotopic equilibration has been first postulated and confirmed by Stewart (1975) by simulating rainfall in a chamber where saturated conditions prevailed. Then, raindrops formed in upper atmospheric levels continuously exchange water molecules with the surrounding water vapor as they fall. These exchanges tend to re equilibrate isotopically the two water phases at each atmospheric level. They are all the more effective the closer the atmosphere is to saturation. In unsaturated air, rain also partially evaporates below clouds. In addition to the aforementioned equilibrium fractionation, the different water molecules diffusivities ($H_2{}^{18}O$ and $HD^{16}O$ diffuse lower than $H_2{}^{16}O$) induce a kinetic isotopic fractionation during water evaporation. From both $\delta^{18}O$ and δD, the deuterium excess parameter is commonly calculated and used to explore processes mainly controlled by kinetic isotopic fractionation. It is defined as (Dansgard ,1964):

$$\mathrm{d} = \delta\mathrm{D} - 8 \cdot \delta^{18}\mathrm{O} \quad (2)$$

The balance between thermodynamic and kinetic processes (and so the isotopic equilibrium state between raindrops and ambient vapor) is influenced by below-cloud relative humidity as well as rain and cloud characteristics (height of condensation, height of melting layer, height of cloud base, droplets size and precipitation rate) (Managave et al., 2016; Wang et al., 2016; Aggarwal et al., 2016). Recycling of evapotranspired moisture from the surface can also prevent the isotopic equilibrium state (Anderson et al., 2002; Aemissegger et al., 2015; Desphande et al., 2010; Lekshmy et al., 2018).

As a consequence, the question of the distance to the isotopic equilibrium for precipitation and water vapor is raised (Stewart, 1975) as it is of large relevance for a set of studies:

- The isotopic equilibrium is an initial hypothesis in a number of modeling studies requiring the isotopic composition of water vapor (δ_v) as a key parameter (Craig and Gordon, 1965): because the observations of δ_v are still few compared to the observations of the isotopic composition of precipitation (δ_p), the later is often used to deduce δ_v based on the equilibrium state;

- The understanding of isotopic exchanges between raindrops and ambient water vapor can offer better constraints on below-cloud atmospheric processes and on the vertical structure of precipitation systems (Bony et al., 2008; Risi et al., 2008; Aemissegger et al., 2015; Lekshmy et al., 2018; Graf et et al., 2019) provided that all processes influencing the rain-water vapor isotopic exchanges can be disentangled (Graf et al., 2019);

- Paleoclimate reconstructions based on archives of δ_p assume that the later is a correct proxy for δ_v (through the isotopic equilibrium), which is itself considered an integrated tracer of all climate processes along air masses trajectory. Post-condensation exchanges in the atmosphere between water vapor and precipitation thus raises the question of the representativeness of δ_p compared with δ_v.

Simultaneous isotopic observations in rain and water vapor are needed to examine whether equilibrium state prevails and, if appropriate, to identify the causes inducing a departure from equilibration. Despite the recent advent of commercial laser absorption spectrometers to measure in situ water vapor isotopic ratios, simultaneous observations of δ_p and δ_v are still limited although in progression (Tremoy et al., 2014; Aemisegger et al., 2015; Graf et al., 2019 for some recent examples). The lack of observations in both water phases is especially apparent in tropical and subtropical environments. Only a few studies have investigated the characteristics of water and rain isotopic ratios in subtropical Northern latitudes where precipitation occur in a summer monsoon context with the following characteristics: large vapor content during saturation at relatively high temperature, potential large contribution of evapotranspiration to surface water vapor, presence of convective and stratiform rains. In West Africa (13.50°N, 2.08°E), Tremoy et al. (2014) explored the rain-water vapor interaction along 74 squall lines during three monsoon seasons (2010, 2011 and

2012). They showed that the isotopic equilibrium state strongly varies from one rain to another and along the monsoon season: precipitation and water vapor are very close to the equilibrium state during the core of the monsoon whereas disequilibrium appears at the beginning and at the end of the rainy season. Evaporation of droplets is the main process involved in isotopic disequilibrium leading to an isotopic enrichment of water vapor at the start of the season (high level of evaporation rate, low relative humidity and enriched precipitation) and to an isotopic depletion of water vapor at the end of the monsoon (lower evaporation rate and very depleted rain). In Southern peninsular India (8.76°N, 77.12°E and 11.51°N and 76.02°E), during the monsoon season, Lekshmy et al. (2018) also showed that disequilibrium between water vapor and rain varies throughout the rainy season with low disequilibrium during the pre-monsoon and the core of the monsoon and higher disequilibrium at the end of the monsoon. They attribute the equilibrium rate to the partition between stratiform and convective precipitation. They argue that during stratiform precipitation vertical mixing can be reduced and below-cloud water vapor can be enriched by transpirated moisture. Further north, in Western India (23.03°N, 72.56°E), Deshpande et al. (2010) and Srivastava et al. (2015) showed that the isotopic equilibrium prevails along the 2007 monsoon except during its onset and retreat. Further southeast, in the Bay of Bengal, in the maritime context of Anadaman Islands (11.66°N, 92.73°E), Sinha and Chakraborty (2020) concluded that water vapor and rain are close to the equilibrium state in average over the entire 2015 Indian monsoon season. In a case study during the 2012 summer season in Taïwan (25.02°N, 121.50°E), Laskar et al. (2014) showed that the isotopic equilibrium state is attained during a typhoon occurring in the late summer monsoon whereas rain and water vapor significantly deviate from the isotopic equilibrium during an equally large rain event earlier in the season. They incriminated long-range transport and high level of isotopic distilation as potential explanations for very depleted rains and thus for a long distance to equilibrium state. In the Chinese subtropics (28°18N, 112.93°E), Yao el al. (2018) showed that water vapor and precipitation are in or near an equilibrium state during the summer monsoon season. Although all these studies explored different tropical and subtropical regions (India, Asia and Africa) with different environment, atmospheric dynamic and climate, they all clearly showed that the isotopic equilibrium state strongly varies throughout the monsoon season and that, most of the time, the equilibrium assumption is fulfilled (or almost fulfilled) during the core of monsoon, i.e when atmospheric conditions are close to saturation with high surface temperatures (>20°C). They also suggest that a large number of processes are involved to explain the equilibrium deviation depending on the site location (type of rain,

below-cloud evaporation of droplets, altitude of condensation, evapotranspiration, variety of the moisture sources and distance of the site to the moisture sources).

To complete these previous studies and to help bridging the knowledge gap in Southern Hemisphere, we present in this paper simultaneous isotopic observations in near-surface water vapor and precipitation in the Bolivian Andes (tropical South America), on two sites at low and high elevation, at the onset and at the end of the 2005-2006 rainy season. Several studies have focused on the controls on δ_p in this Andean region from subseasonal to interannual timescale and on the potential of δ_p for paleoclimate reconstructions (Vimeux et al., 2005; Vuille and Wener 2005; Vimeux et al., 2011; Guy et al., 2019). They concluded that the main control of δ_p is the degree of rainout upstream the Andes, along air masses trajectories, and that the local amount effect is a poor factor in controlling δ_p. Vimeux et al. (2011) and Guy et al. (2019) also reported deuterium excess observations in rain (d_p). They did not conclude on what are the meteorological controls on d_p but they noticed that no relationship appears between d_p and moisture origins and pathways. However, isotopic exchanges between rain and water vapor, their interest in examining atmospheric processes and their potential influence on the climate information contained in δ_p have never been investigated there.

A description of the sites, of the instrumental setup and of isotopic analyses is done in section 2. Methodology is detailed in section 3. Section 4 describes the isotopic observations and the equilibrium state between water vapor and rain. In section 5, we explore to what extent local processes deviate rain and water vapor from the isotopic equilibrium. Further, we examine in which extent δ_p is a correct proxy of δ_v (section 6).

2- Precipitation and water vapor sampling during the 2005 and 2006 field campaigns

2-1 Sampling sites

Water vapor and precipitation were collected simultaneously at two sites in the Zongo Valley (Bolivian Andes): at Huaji (16°02'28"°S, 67°58'38"°W, 945 m, at the base of the valley) and at Plataforma (16°16'55"°S, 68°07'17"°W, 4750 m, at the top of the valley) (Figure 1). This valley belongs to the Bolivian Company of Electric Energy (COBEE) providing electric power for La Paz (capital city of Bolivia). Pluviometers and water vapor collection systems are located nearby the hydropower plants. The distance between the two

stations is about 30 km as the crow flies (~40 km by road). This valley is located on the northeast side of the Bolivian Cordillera Real and links up the Amazon basin with the Andean summits at the latitude of La Paz (Figure 1). The atmospheric circulation in tropical South America is characterized by easterly trade winds which transport moisture from the Atlantic Ocean and from the central Amazon region toward the eastern Andes. The later act as a barrier and deviate the moisture flow parallel to the Andes toward the southern Amazon and the subtropical region of South America (the so-called South American Low-Level Jet (SALLJ) (Marengo et al., 2004). At the synoptic-scale, a southwesterly direction low level air flow, associated to the SALLJ structure, penetrates in the Andes through the east valleys (Vimeux et al., 2011; Junquas et al., 2018) (Figure 1). The orography of the valleys locally strengthens this moisture transport by both mechanical channelization of the moisture flux and thermally driven surface upslope flow developing along the Amazon slopes (Junquas et al., 2018). The uplift of air masses can be reduced or reversed during nighttime in the upper part of the valleys because of downslope flows induced by katabatic winds (Junquas et al., 2018). This nighttime reverse moisture flow is probably unusual in the Zongo valley during the rainy season (Junquas et al., 2018) as supported by the uniformity of the isotopic composition of precipitation along the valley regardless of rainy hours (Vimeux et al., 2011). There are however a few exceptions: some punctual isotopic discrepancies can be seen in precipitation between Huaji and Plataforma. They are attributed to a westerly flow from the Bolivian Altiplano (Vimeux et al., 2005, 2011) that can develop during weak easterly winds and reaches the top of the valley. This diurnal local atmospheric circulation is also supported by a 1 km-resolution simulation of moisture flows around the Zongo valley carried out with the WRF model (Weather Research and Forecasting model) (C. Junquas and J-P. Sierra, pers. comm.).

We chose to sample rain and water vapor at these two extreme locations in this valley for different reasons. First, we wanted to examine the water vapor-rain interactions at locations undergoing different meteorological conditions (temperature and relative humidity, Table 1). Indeed, the atmosphere at Huaji is always very close to saturation conditions from October to April and diffusive exchanges are expected to dominate rain-water vapor interactions. In contrast, lower relative humidity at Plataforma could promote evaporation of droplets under the cloud although temperature is very low (Table 1). Secondly, different types of surface are encountered at the two sites. Vegetation dominates at Huaji while bare soil is present at Plataforma. In addition, Huaji site is close to the Zongo stream resulting in a

206 possible secondary moisture source. As a result, an evapotranspired moisture flux could be
207 encountered at Huaji unlike Plataforma. At Plataforma, the site is at about 130 m from the
208 Zongo water reservoir, at the base of the Zongo glacier (16°16'S, 68°09'W, from 4900 to 6000
209 m), in which glacier runoff is stored by COBEE. The lake reservoir can potentially evaporate
210 and contribute to local humidity. However, given the mean temperature at this site during our
211 field campaigns (~2°C), this water body is unlikely to be a significant source of surface water
212 vapor relative to the ascent of moisture from the base of the valley. Then, event-based and
213 monthly rains have been sampled at both sites for isotopic analyses since 1999 (Vimeux et al.,
214 2005, 2011). The proximity of the COBEE hydropower plants allowed us to have dedicated
215 observers monitoring the pluviometers since 1999, guaranteeing the quality of the
216 observations. Thus, we only needed to set up the water vapor collection at a few meters from
217 pluviometers. At last, the available precipitation data in this valley over several years allowed
218 us to characterize the 2005-2006 rainy season comparatively to the other years.

219 Two field campaigns were organized at the onset (October-November) and at the
220 termination (March-April) of the 2005-2006 wet season. We chose those transition periods as
221 they are supposed to offer (1) a sufficient atmospheric moisture level to collect enough water
222 vapor within ~24h for mass spectrometer analyses and (2) a balance between time periods
223 with atmospheric conditions close to saturation within the heart of the rainy season (when
224 diffusive exchanges are supposed to control isotopic processes leading to the equilibrium) and
225 time periods with only a few rain events, during the start and the end of the dry season, with
226 lower surface relative humidity (when evaporative processes under clouds are supposed to
227 take place). During the first campaign, water vapor sampling started on October 23rd, 2005 at
228 both stations and ended on November 21st, 2005 (November 27th, 2005) at Huaji
229 (Palataforma). The second campaign started on March 15th, 2006 (March 11st, 2006) and
230 ended on May 1st, 2006 (April 30th, 2006) at Huaji (Plataforma).

231 **2-2 Water vapor and rain collection**

232 Water vapor was collected using the cryogenic technique described for example in
233 Yakir and Wang (1996), or Yakir and Sternberg (2000) (laser instruments based on
234 Wavelength-Scanned Cavity Ring Down Spectroscopy (WS-CRDS) (Gupta et al., 2009) were
235 not available in 2005-2006). The two cryogenic systems drew air from an intake at about ~2.5
236 m above the surface through a heated PFA (perfluoroalkoxy) tubing to avoid any
237 condensation. The length of the heated tubing between the inlet and the cold trap was about 3

m. The cold trap was immerged in ethanol-dry ice maintained at about -90 °C using a cryocooler (Thermo Scientific HAAKE EK 90 model). The cold trap was made up of two parts: the main trap was a Pyrex spiral double trap and a secondary Pyrex spiral single trap was placed right after to check that all water vapor was captured. The air flow-rate was regulated at ~45L/hour to avoid any ice plug at the entrance of the main trap (at Plataforma). A KNF pump (N86 KN.18 model) was placed on the outlet line. For each campaign, the two cryogenic systems used at Huaji and Plataforma were tested by simultaneously collecting water vapor during one week at Huaji before the beginning of the campaign and were validated by comparing isotopic results. In order to capture enough water vapor volume for mass spectrometer analyses, water vapor was collected during time periods from 14h to 31h with a majority of collections around 23h. All the iced water samples were recovered into liquid water on site. Water volumes varied between 1 ml (at Plataforma) up to ~20 ml (at Huaji). Precipitation was collected at the two stations on an event-based resolution, immediately after the rain event as described in Vimeux et al. (2011).

2-3 Isotopic analyses and on site meteorological measurements

In 2005, 23 (30) water vapor samples and 26 (30) precipitation events were collected at Huaji (Plataforma). The second field campaign in 2006 was longer and 42 (41) water vapor samples and 48 (40) precipitation events at Huaji (Plataforma) were collected. Both $\delta^{18}O$ and δD and were measured on water vapor and precipitation by mass spectrometers (Finnigan MAT 252 coupled with the usual CO_2-H_2O equilibration for $\delta^{18}O$ and LSCE home-made mass spectrometer coupled with water reduction on 600°C-heated uranium for δD) except for some water samples with volumes lower than 3 ml. In that case, we were not able to measure $\delta^{18}O$ (samples are now empty and they cannot be measured with a WS-CRDS laser analyzer requiring smaller water volumes). This situation occurred for example for a number of Plataforma water vapor samples during 2005 and 2006. The other gaps in water vapor isotopic ratios record correspond to days for which the cryogenic system had technical problems. The accuracies of measurements are of ±0.5‰ and ±0.05‰ for δD and $\delta^{18}O$ respectively, leading to an average quadratic analytical uncertainty on d lower than ±0.7 ‰ for both phases (hereafter, d_v and d_p for water vapor and precipitation respectively).

During both campaigns, 10-min resolution surface temperature and relative humidity were recorded using a HOBO® sensor from Onset Computer Corp at Huaji. At Plataforma, 30-min surface temperature and relative humidity were recorded by a meteorological station

on site (TRIES-CLIMA model).

3- Methodology

3-1 Calculation of the distance to the isotopic equilibrium

In this paper, we explore how far from the isotopic equilibrium with surrounding water vapor are the raindrops. As a consequence, the isotopic disequilibrium (ΔD_{p_eq}) is defined as the difference between the observed δD_p and the calculated isotopic composition of precipitation at equilibrium with water vapor (δD_{p_eq}) as:

$$\Delta D_{p\_eq} = \delta D_p - \delta D_{p\_eq} \quad (3)$$

where δD_{p_eq} is calculated according to:

$$\alpha_{eq} = \frac{\delta D_{p\_eq} + 1000}{\delta D_v + 1000} \quad (4)$$

where α_{eq} (>1) is the precipitation-water vapor equilibrium fractionation coefficient (Majoube, 1971).

For each δD_v measurement, we examine whether rain occurred during the collection of water vapor. If this is the case, $\alpha_{eq,}$ is calculated considering the average temperature over the rain event considered, of composition δD_p . When several rain events occurred during the time period of water vapor collection, temperature is averaged over the different rain events to calculate α_{eq} and the amount-weighted δD_p is used in Equation (3).

In addition to ΔD_{p_eq}, we similarly define Δd_{p_eq} accounting for the disequilibrium relative to deuterium excess as:

$$\Delta d_{p\_eq} = d_p - d_{p\_eq} \quad (5)$$

The definition of ΔD_{p_eq} offers the possibility to review processes potentially involved in departure from equilibrium state based on the sign of ΔD_{p_eq}: a negative disequilibrium suggests that precipitation is more depleted than a condensate that would have been formed from surface water vapor and in contrast a positive disequilibrium suggests that precipitation is more enriched than expected at equilibrium. The combination of ΔD_{p_eq} and Δd_{p_eq} provides an original metric to discuss below-cloud atmospheric processes as used by Graf et al. (2019)

(see section 3-2).

3-2 Below-cloud evaporation and diffusion processes

When raindrops fall through the atmosphere in unsaturated conditions, they experience evaporation with kinetic fractionation and they partially (or fully) re equilibrate by diffusion with the ambient vapor. The isotopic exchanges that take place between falling drops and water vapor through evaporation and diffusion processes are treated in a unified manner in the Stewart's theory (Stewart, 1975).

We consider a droplet (P_0) in the cloud with an initial mass m_{p0} of isotopic ratio R_{p0}, in equilibrium with cloud water vapor of isotopic ratio R_{v0}, falling into an air of isotopic ratio R_v. R_v is actually the surface isotopic ratio assuming a strong mixing layer under the cloud where evaporation proceeds. R_{p0} is typically more depleted than the precipitation at the isotopic equilibrium with R_v so that $R_{p0}<\alpha_{eq}R_v$. As raindrop evaporation proceeds, we note m_p the rain mass and we define the residual fraction of liquid, f, as:

$$f = \frac{m_p}{m_{p0}} \quad (6)$$

As a consequence, the parameter f varies from 1 (no evaporation) to 0 (total evaporation).

The precipitation isotopic ratio R_p is given as a function of f by Stewart et al. (1975):

$$R_p = f^{\beta} \cdot R_{p0} + (1 - f^{\beta}) \cdot \gamma \cdot R_v \quad (7)$$

where β and γ coefficients are defined as:

$$\beta = \frac{1 - \alpha_{eq} \cdot (1 - h) \cdot \left({}^{D}/_{D'}\right)^{n}}{\alpha_{eq} \cdot (1 - h) \cdot \left({}^{D}/_{D'}\right)^{n}} \quad (8)$$

$$\gamma = \frac{\alpha_{eq} \cdot h}{1 - \alpha_{eq} \cdot (1 - h) \cdot \left({}^{D}/_{D'}\right)^{n}} \quad (9)$$

where D/D' is the ratio of molecular diffusivities in air of the most ($H_2{}^{16}O$) and less ($H_2{}^{18}O$ or $HD^{16}O$) abundant isotopologues (1.0285 and 1.0251 for $H_2{}^{18}O$ and $HD^{16}O$

respectively) (Merlivat, 1978), n is a parameter that modulates the water molecules diffusivity and that depends on drop size and h is the ambient relative humidity. In our calculations, the n parameter is set to 0.58, corresponding to droplets of 1 mm in diameter (Stewart, 1975; Bony et al., 2008).

The Stewart's theory assumes that all the droplets have the same size and that the water vapor isotopic ratio is not too much affected as evaporation proceeds.

Some consequences arise from the Stewart's Equation (7):

(1) As evaporation proceeds, raindrop gets enriched and its deuterium excess decreases (because HDO diffuses faster than $H_2{}^{18}O$). R_p in Equation (7) tends to a target value of $R_{p\_target} = \gamma R_v$ (f=0). The lower the relative humidity, the higher the target value. This implies that if evaporation and diffusive processes explain ΔD_{p_eq}, the later has a maximal value of $1000(\gamma - \alpha_{eq})R_v$ attained for f=0. The dryer the air is, the more strongly the maximum ΔD_{p_eq} can take positive values. Similarly, d_p tends to a target value for f=0 (the lower the relative humidity, the lower the target value) and Δd_{p_eq} has a minimal value attained for f=0.

(2) As evaporation proceeds, the distance of the observations to the target value is given by $1\text{-}f^{\beta}$. For example, for f^{β}=0.2, 80% of the distance between the isotopic composition of P_0 and the one of the target precipitation (P_{target}) is achieved. The path to the target is traveled all the more efficiently as the evaporated fraction is strong (weak f) and as h is strong (in this case, diffusive exchanges are favored and β has high values).

The quantity f^{β} in equation (7) can be written in delta notation as:

$$f^{\beta} = \frac{\delta D_p - \delta D_{p\_target}}{\delta D_{p0} - \delta D_{p\_target}} \quad (10)$$

f^{β} is calculated here considering δD. It can also be calculated from $\delta^{18}O$. The two results are very close each other as f^{β} is mainly controlled by f and h. Under such conditions, we assume in our study that:

$$f^{\beta} = \frac{\delta D_p - \delta D_{p\_target}}{\delta D_{p0} - \delta D_{p\_target}} = \frac{d_p - d_{p\_target}}{d_{p0} - d_{p\_target}} \quad (11)$$

Therefore, if evaporation and diffusion are the unique processes at play, Equation (11) applies with a unique initial precipitation P_0 and f can be calculated. Consequently, in our study, for each disequilibrium considered, we seek whether there exists a unique P_0 satisfying Equation (11). As done for example in Graf et al., (2019), P_0 can be estimated in a diagram representing Δd_{p_eq} as a function of ΔD_{p_eq} so that the three precipitation P_0 (f=1), P (the observation) and P_{target} (f=0) are aligned (see Figure 2 and its legend for explanations). Then, f^{β} and f can be graphically deduced (or calculated).

The previous calculations are not defined at saturation (h of 100%, pure diffusive case). In that case, there is virtually no evaporation and diffusive exchanges dominate between raindrop and water vapor as to drive the two phases toward isotopic equilibrium.

3-3 Estimation of local versus large-scale processes influence on δ_p

The partition between local and large-scale effects on water vapor and precipitation isotopic ratios is examined in this paper using the Risi et al. (2010)'s methodology. It relies on the hypothesis that the isotopic composition of water vapor further reflects large-scale processes affecting the air masses along its trajectory (e.g. isotopic distillation, vertical mixing induced by convection and large-scale subsidence), whereas the isotopic composition of precipitation can be affected by local processes such as evaporation of droplets. This method does not allow us to discuss the type of local processes involved in the δD_p departure from δD_v (or δD_{p_eq}) but it determines how much local effects affect δD_p. Variations of the later are decomposed into a large-scale processes contribution (δD_v) and a local processes contribution (δD_p - δD_v) as follows:

$$\delta D_p = \delta D_v + (\delta D_p - \delta D_v) \quad (12)$$

Based on Equation (12), we can say that the contribution of large-scale processes to δD_p can be estimated by the slope (a) of the linear regression of δD_v as a function of δD_p:

$$\delta D_v = a \cdot \delta D_p + b \quad (13)$$

Similarly, the contribution of local processes to δD_p can be estimated by the slope (c) of the linear regression of $\delta D_p - \delta D_v$ as a function of δD_p:

$$\delta D_p - \delta D_v = c \cdot \delta D_p + d \quad (14)$$

This decomposition leads to:

$$\delta D_p = a \cdot \delta D_p + c \cdot \delta D_p \quad \text{with } a + c = 1 \text{ and } b = -d \quad (15)$$

For example, if large-scale (local) processes fully explain δD_p, the value of a (c) will be 1 (0) and the value of c will be 0 (1).

A similar decomposition method can be applied for deuterium excess, with a large-scale processes contribution (d_v) and a local processes contribution (d_p - d_v).

As in section 3-1, in order to compare the isotopic composition of water vapor and precipitation, we have considered rain event(s) occurring within the period of water vapor sampling. When several rain events occurred during the time period of water vapor collect the amount-weighted δD_p is used.

4- Results

4-1 Precipitation

We compared monthly precipitation amount during the 2005-2006 rainy season (i.e. from October 2005 to April 2006) with monthly precipitation amount averaged over the rainy seasons from 2000 to 2011 (from October to April). For this purpose, we used data from 5 monthly pluviometers well stacked from the base to the top of the Zongo valley (Figure 1 and Vimeux et al., 2005). At each station, the total precipitation from October 2005 to April 2006 is higher by 1.8 to 20.0% compared to the 2000-2011 period (Figure 3a). For each month, from October 2005 to April 2006, total precipitation over the valley (sum of precipitation amount over the 5 stations) is higher by 11.0 to 46.6% compared with the mean total precipitation over 2000-2011, except in February and April 2006 where total precipitation is lower by 35% and 1% respectively (Figure 3b). Regarding the occurrence of precipitation events, the 2005-2006 rainy season exhibits a significant number of precipitation events from March to April 2006 (+190 and +360% of rain events at Huaji and Plataforma respectively compared with averaged March-April period over 2000-2011).

During the two campaigns, we observed orographic rains that develop along the Zongo valley slope, without convection. Consistently, precipitation rates are low (Table 1). Focusing only on the rain events that occured during water vapor sampling, precipitation rates varied from 0.1 to 16 mm/h (80% of rain events exhibit a precipitation rate lower than 5mm/h

and only 4 events have rain rates higher than 10 mm/h) with a mean (median) of 3.5 (2.2) mm/h. The 68%-confidence interval is between 0.8 and 6 mm/h (precipitation rate follows a log-normal distribution).

4-2 δD_p and δD_v at Huaji and Plataforma

During the 2005 and 2006 campaigns, the range of δD_v at Huaji (Plataforma) is -76.7 to -167.4‰ (-101.6 to -233.3‰) with a mean of -121.9±22.6‰ (-163.6±33.6‰), whereas the range of δD_p is -3.5 to -131.0‰ (-9.3 to -201.7‰) with a mean of -63.0±32.7‰ (-111.7±46.1‰) (Figure 4). Distinctions between the onset and the end of the rainy season are reported in Table 1. We see that for both water phases, in average, the isotopic depletion is higher in 2006 than in 2005. This can be explained by the seasonal progressive isotopic discharge of water vapor along the rainy season due to the cumulative local and upstream rainout as shown by Vimeux et al. (2005, 2011) and Vuille and Werner (2005).

During the two campaigns, we collected water vapor during time periods with no rain and conversely, a few rain events occurred while the water vapor system was not operational. Therefore, 70 simultaneous observations of δD_p and δD_v are available at Huaji (37 observations) and Plataforma (33 observations). δD_p and δD_v clearly evolve in parallel at both sites over the whole period: covariances (r^2) are 0.87 (n=37) and 0.83 (n=33) respectively at Huaji and Plataforma ($p<0.001$).

4-3 d_p and d_v at Huaji and Plataforma

As for deuterium, deuterium excess exhibits fluctuations both in water vapor and in precipitation during the 2005 and 2006 campaigns. The range of d_v at Huaji (Plataforma) is 10.8 to 17.3‰ (12.5 to 26.1‰) with a mean of 14.4±1.7‰ (20.6±3.6‰), whereas the range of d_p is 1.6 to 15.4‰ (10.8 to 22.9‰) with a mean of 10.2±2.9‰ (16.6±2.7‰). On both sites, we observe that averaged deuterium excess in water vapor is higher than in precipitation by ~4‰ (4.2‰ and 3.9‰ at Huaji and Plataforma respectively) (see the sign of d_p-d_v on Figure 4). On both sites, we also observe that the mean d_p is slightly higher in 2005 than in 2006 (Table 1). However, the mean d_v at Huaji are similar in 2005 and 2006 whereas at Pataforma, the mean d_v is lower in 2005 than in 2006 (Table 1).

Because of missing $\delta^{18}O_v$ (mainly at Plataforma, see section 2), only 54 (and not 70) simultaneous observations of d_p and d_v are available at Huaji (35 observations) and

Plataforma (19 observations). Covariances between d_p and d_v are much lower than between δD_p and δD_v and falls to 0.17 (n=35) and 0.02 (n=19) for Huaji and Plataforma respectively. However, variations of d_p reflects those of d_p-d_v with covariances of 0.65 (n=35) and 0.56 (n=19) at Huaji and Plataforma respectively.

4-4 Comparison between Huaji and Plataforma

δD_v exhibits similar variations at Huaji and Plataforma (the slope of the linear regression between δD_v at Huaji and Plataforma is of 1.03, r^2=0.59, n=54, p<0.001) except during one week in November 2005 (between November 8th and 15th), a few days in mid-March 2006 (between 13th and 18th March) and in April 2006 (between April 6th and 10th) (Figure 4). Without accounting for those periods of discrepancies, the covariance of δD_v between the two sites increases to 0.75 (n=43, p<0.001) with a significant difference between the onset (r^2=0.79, n=17, p<0.001) and the termination (r^2=0.34, n=26, p<0.01) of the wet season.

Similarly to δD_v, δD_p exhibits similar variations between Huaji and Plataforma (the slope of the linear regression between δD_p at Huaji and Plataforma is 1.05, r^2=0.64, n=31, p<0.001). The aforementioned discrepancies on δD_v between Huaji and Plataforma are also recorded in δD_p, and by skipping those rainout events the covariance between the two sites increases up to 0.73 (n=21, p<0.001) with again a significant difference between the onset (r^2=0.96, n=7, p<0.001) and the termination (r^2=0.50, n=14, p<0.01) of the wet season.

In this paragraph, we explore if the aforementioned isotopic discrepancies between the two sites could reflect different moisture sources at Plataforma and Huaji on these specific days. Indeed, as mentioned in section 2-1, a persistent moisture flow from the Bolivian Altiplano could impact Plataforma station and not Huaji. Interestingly, we can compare δD_p at Plataforma with δD_p of event-based precipitation collected at Layca Cota (a site located downtown La Paz on the Altiplano, at 16°30'16"S and 68°07'23"W, 3635 m, and thus on the western Andean side) where δD_p has been monitored since December 2001 (Figure 4). The two signals are fairly similar from November 8th to 15th, 2005 and during mid-March 2006 although there are only two common days between the two isotopic series during this period (there is no precipitation at Layca Cota in April 2006). This similarity suggests that Plataforma and Layca Cota stations sample over these specific time periods similar air masses that do not attain the Huaji station. As an initial exploration, we used the HYSPLIT

backtrajectory model (Draxer and Rolph, 2010; Rolph, 2010) to calculate air masses pathways for those specific days. This model runs with the 1°-resolution operational NCEP-GDAS (National Centers for Environmental Prediction-Global Data Assimilation System) analyses. This resolution is too low to distinguish Palataforma and Huaji sites. However, it allows us to examine the main large-scale direction from which air masses originate and thus to distinguish a potential moisture arrivals from the Bolivian Altiplano. From November 8th to 16th, 2005, the remote air parcel origin (>4 days) is located southward indicating long air masses pathways at mid-latitudes (Ronchail et al., 1989) consistent with a strong isotopic distillation (δD_p from November 8th to 15th, 2005 are among the most depleted values). When air masses approach the latitude of La Paz and of the Zongo valley, they are northwestward transported, certainly not overflying the low elevation of the Zongo valley. As a consequence, the periods of discrepancies in δD_p between Huaji and Plataforma may be due to different air masses origin and history between the two sites. Plataforma would have experienced air masses originating from the highlands, affecting the highest summits of the Cordillera and barely passing over them as already observed in this area between November and March for the very close site of Chacaltaya atmospheric platform (16°21'1.78"S, 68°8'53.44"W, 5240 m, at about 8 km from Plataforma station, Figure 1) (Andrade et al., 2016; Wiedensohler et al., 2018). This local air flow circulation between the Bolivian Altiplano, the high summits of the Cordillera Real and the top of the Zongo valley would need to be confirmed by higher resolution models. It is worth noting that deuterium excess in both precipitation and water vapor for those days does not exhibit a specific signature that could be associated to the southward moisture origin. This lack of signal in d_p for southward moisture origin has already been pointed out by Vimeux et al. (2011). Guy et al. (2019) also observed in several Bolivian and Peruvian rain isotopic ratios series in the Andes that no relationship appears between extreme d_p and large-scale moisture sources and trajectories.

The variations of d_v at Huaji and Plataforma show similarities although the relationship is lower than for δD_v (the slope is of 0.99, r^2=0.33, n=19, $p<0.05$) whereas a less significant relationship is shown for d_p (r^2=0.14, n=31, $p<0.05$) suggesting that local effects may affect d_p.

4-5 Altitudinal isotopic gradients

As water vapor and rain isotope ratios are reported for two elevations, we give here the main features of the isotopic altitudinal gradient. As expected, water vapor and precipitation

isotopic ratios at Plataforma are more depleted than at Huaji. The mean δD_v difference between the two sites is of -38.2±16.5‰ (this value is calculated only over common days of water vapor sampling and does not account for the aforementioned discrepancies in δD_v between the two sites). This leads to a mean isotopic-altitude gradient of -1.0‰/100m. A similar isotopic gradient is found for precipitation (-1.3‰/100m). Those results are consistent with previous calculations done in Vimeux et al. (2005, 2011) along the Zongo valley from monthly and event-based precipitation isotope ratios over longer periods. We observe a similar gradient in the water vapor phase at the onset and at the termination of the wet season (-0.8‰/100m in 2005 and -1.1‰/100m in 2006). This similarity is also observed on precipitation (-1.2 and -1.3‰/100m in 2005 and 2006 respectively). The altitudinal isotopic gradient is commonly attributed to the orographic rainout effect along the Andean slopes. It can also arise from shallow convection that allows for free troposphere and boundary layer air masses mixing along Andean slopes, and that depletes surface water vapor at high altitude (Angert et al., 2008; Welp et al., 2012; Bailey et al., 2013; Guilpart et al., 2017). However, this last assumption is not favored here. First, the similarity of δD_p and δD_v between the base and the top of the valley (also seen in Vimeux et al., 2011) suggests that most of the time the same air mass travels and precipitates from the base to the top of the valley. Second, we clearly did not observe convection during the field campaigns.

We also observe a strong effect of the altitude on d_v with higher values at Plataforma than at Huaji. The mean gradient is +0.2‰/100m (n=19). The same gradient is observed on d_p (n=31). No difference is seen between the onset and the termination of the rainy season. This gradient for deuterium excess may arise from the complete discharge of air masses as they are lifted up to the summit of the valley: as δD_v decreases, and in an idealized case tends to -1000‰ for both isotopes as the end of Rayleigh isotopic distillation, d_v tends toward +7000‰ per definition. In addition, vertical mixing between free troposphere and boundary layer may contribute to increase d_v in altitude. Actually, high d_v values can prevail in the upper atmosphere due to ice crystal formation (Jouzel and Merlivat, 1984) or to the influence of remote deep convection (Bony et al., 2008). However, our understanding of the local atmospheric circulation in the Zongo valley does not support the presence of intense vertical mixing of air in the upper part of the valley.

4-6 Isotopic disequilibriums

ΔD_{p_eq} is calculated for 70 simultaneous observations of δD_p and δD_v at Huaji (37

observations) and Plataforma (33 observations). ΔD_{p_eq} varies from -51.5 to 35.0‰. ΔD_{p_eq} is mostly negative (73%) and the mean of negative ΔD_{p_eq} is -17.5‰ (positive and negative ΔD_{p_eq} do not follow a normal distribution and so no standard deviation is calculated, see ΔD_{p_eq} distribution on Figure 5a and b). The positive ΔD_{p_eq} reflect a lower departure from the isotopic equilibrium with a mean of 4.8‰.

The distribution of ΔD_{p_eq} is significantly different at Huaji and at Plataforma (Figure 5a). At Huaji (Plataforma), the mean negative ΔD_{p_eq} is of -9.6‰ (-24.1‰) representing 62% (85%) of the ΔD_{p_eq}. Plataforma also records the most negative disequilibriums (100 (83)% of the ΔD_{p_eq} lower than -20 (-30)‰ are encountered at that site) whereas the positive ΔD_{p_eq} are mainly observed at Huaji (74%). This relationship between the sign of ΔD_{p_eq} and the two sites is significant at the 95%-confidence level according to a Chi-squared test. In addition, the mean absolute distance to the isotopic equilibrium at Huaji (Plataforma) is 7.7‰ (21.2‰) and 70% (27%) of ΔD_{p_eq} range from -10‰ to +10‰. ΔD_{p_eq} is thus more pronounced at Plataforma than at Huaji and exhibits a deviation towards negative values.

By examining the differences between 2005 and 2006 (Figure 5b), we note that the number of positive (negative) ΔD_{p_eq} is similar in 2005 and 2006 (29(71) and 26(74)% respectively) although we observe that the four most positive ΔD_{p_eq} (5.0‰, 7.2‰, 16‰ and 35.0‰) occur in 2005 whereas the lowest ΔD_{p_eq} (<-50‰) can be observed during the two campaigns.

We captured at Huaji 17 rain events with an averaged relative humidity of 100%. Although we can expect that the equilibrium state prevails in saturation conditions, ΔD_{p_eq} is not equal to 0 and can be positive or negative (ΔD_{p_eq} <0 for 11 rain events). We observe that the mean absolute distance to isotopic equilibrium for those 17 rain events is 8.2‰, similar to the mean absolute distance over the whole dataset at this station (7.7‰).

Regarding how ΔD_{p_eq} varies along with other observations, it is worthwhile noting that:

(1) ΔD_{p_eq} and relative humidity (<100%) do not co-vary (r^2=0.06, n=50, p<0.1). The correlation hardly increases up to r^2=0.10 (n=12, p<0.1) if considering only positive ΔD_{p_eq} ($\delta D_p > \delta D_{p\_eq}$). This suggests that processes dependent on relative humidity and increasing δD_p relatively to its value at equilibrium are not dominant;

(2) a significant positive relationship is observed between ΔD_{p_eq} and δD_p with a covariance of r^2=0.30 (n=70, p<0.001) suggesting that processes enhancing the deviation from equilibrium towards negative values ($\delta D_p < \delta D_{p\_eq}$) tends also to deplete δD_p (Figure 5c).

Δd_{p_eq} is calculated over 54 simultaneous observations of d_p and d_v at Huaji (35 observations) and Plataforma (19 observations) (Figure 6). It varies from -11.3 to 2.4‰. It is mostly negative (78%) and the mean of negative Δd_{p_eq} is -3.3‰. The positive Δd_{p_eq} occur at Huaji (except for one Δd_{p_eq}<0 at Plataforma) and reflect a lower departure from the isotopic equilibrium with a mean of 0.9‰ (Figure 6). Because of missing Δd_{p_eq} at Plataforma in 2005, we do not compare in details the two sites and the two campaigns. No significant correlation is found between Δd_{p_eq} and other isotopic and meteorological parameters.

Interestingly, although deviations from isotopic equilibrium appear at the individual rain event scale, the covariance between δD_p and δD_{p_eq} for the whole dataset is highly significant (r^2=0.86 over the whole data set with r^2=0.85 and r^2=0.83 for Huaji and Plataforma respectively, p<0.001). This suggests that the isotopic equilibrium is a more robust assumption at the subseasonal scale (several weeks) than for individual rain events as already pointed out by previous studies (Deshpandes et al., 2010; Srivasta et al., 2015; Lekshmy et al., 2018; Penchenat et al., 2020). The covariance between d_p and d_{p_eq} over the whole dataset, although lower (r^2=0.56) is also highly significant (p<0.001).

5- How are local processes involved in vapor-rain isotopic disequilibrium?

Our observations show that equilibrium state between water vapor and rain does not prevail during our campaigns at the individual rain scale. The range and the sign of disequilibriums, as well as the different conditions of relative humidity and temperature during the two campaigns, suggest that a variety of processes are at play during isotopic exchanges between rain and water vapor. In this section, we review local processes possibly involved in the isotopic disequilibrium between rain and vapor. In a first part (section 5-1), we propose a metric to estimate the potential errors made on the calculated disquilibriums because of the different time duration in rain and water vapor collection.

5-1 Errors on calculated disequilibriums due to water vapor sampling

An important caveat in our study deals with the difference in the duration of water vapor and rain sampling periods. Water vapor was collected for time periods ranging between

14h to 31h, with a majority around 23h, whereas precipitation samples correspond to specific rain event(s) never exceeding a few hours. This difference in sampling time periods was common before the advent of laser spectrometry and is still present in a few recent studies (Kurita et al., 2013; Lekshmy et al., 2018; Sinha and Chakraborty, 2020).

Before exploring physical processes that could be involved in isotopic disequilibriums, we propose in this sub section to estimate the error that may affect ΔD_{p_eq} (ε_D) and Δd_{p_eq} (ε_d) if the isotopic composition of water vapor is different during and outside the rain event. This estimate could thus be reused in future studies facing the same concern or for example in studies where rain hours are not well know (Penchenat et al., 2020).

The isotopic composition of water vapor before and after the rain event is noted δD_{v_out} and d_{v_out}. The isotopic composition of water vapor during the rain event is noted δD_{v_ev} and d_{v_ev}. We define X_D and X_d the differences of the isotopic composition of water vapor between inside and outside the rain event as:

$$X_D = \delta D_{v\_ev} - \delta D_{v\_out} \quad (16)$$

$$X_d = d_{v\_ev} - d_{v\_out} \quad (17)$$

If the isotopic composition of water vapor decreases during rain event then $X_D<0$ and if deuterium excess increases during the rain event then $X_d>0$, and conversely.

We define r as the fraction of the full water vapor sampling period (of composition δD_{v_ave} and d_{v_ave}) that is during the rain event. In our manuscript, we try to estimate the disequilibrium $\Delta D_{p\_eq\_ev}$ (δD_p - $\delta D_{p\_eq\_ev}$), which was not measured, by $\Delta D_{p\_eq\_ave}$ (δD_p - $\delta D_{p\_eq\_ave}$), which was measured. In the Supplementary Material, we demonstrate that the errors ε_D ($\Delta D_{p\_eq\_ave}$ - $\Delta D_{p\_eq\_ev}$) and ε_d ($\Delta d_{p\_eq\_ave}$ - $\Delta d_{p\_eq\_ev}$) can be written as:

$$\varepsilon_D = \alpha_{eq\_D} \cdot (1 - r) \cdot X_D \quad (18)$$

$$\varepsilon_d = (1 - r) \cdot ((\alpha_{eq\_D} - \alpha_{eq\_18O}) \cdot X_D + \alpha_{eq\_18O} \cdot X_d) \quad (19)$$

We note that the ratio, $\varepsilon_D/\varepsilon_d$, does not depend on r and is equal to:

$$\frac{\varepsilon_d}{\varepsilon_D} = \frac{\alpha_{eq\_D} - \alpha_{eq\_18O}}{\alpha_{eq\_D}} + \frac{\alpha_{eq\_18O}}{\alpha_{eq\_D}} \cdot \frac{X_d}{X_D} \quad (20)$$

In our study, the fraction r is rather well known and about 10% (i.e. a water vapor

sampling period of 23h and a rain event of 2h). To quantify ε_D and ε_d, we also need to estimate the range of X_D and X_d. To this purpose, we would ideally need to refer to continuous high resolution water vapor isotopic observations in tropical and subtropical regions before, during and after rain events. Such observations have been published for cyclonic rains. However, this type of rain differs too much from the orographic rain encountered in the Zongo valley to be considered. Tremoy et al. (2014) in West Africa is so far the only study that has examined changes in water vapor and rain isotopic composition during rain events at a 5-minute time resolution and in a subtropical climate. Although rain events are mostly convective rain, this study offers some upper bound values for X_D and X_d. They showed that for 80% of rain events, average $\delta^{18}O_v$ during rain interval is depleted by 1 to 2‰ compared with $\delta^{18}O_v$ averaged over the 30-min time interval preceding the rain start. The last 20% of rain events show an average increase of $\delta^{18}O_v$ of about 0.8‰ during rain event. Tremoy et al. (2014) showed also that the average d_v over rain events is higher during all studied rain events by 0.5 to 2.3‰ compared with mean d_v over the 30-min time interval preceding the rain start. Tremoy et al. (2014) attributed this d_v increase to rain evaporation. Based on these amplitude changes for $\delta^{18}O_v$ and d_v during rain events, we determine changes in δD_v during the rain event (i.e X_D varies from -15 to 10‰) and we simulate the errors ε_D and ε_d for 3 values of X_d (0‰, 0.5‰ and 2‰) with a fraction r of 0.1. The ε_D and ε_d co-variation is plotted on Figure 6. We clearly see on this figure that:

(1) Errors on ΔD_{p_eq} and Δd_{p_eq} positively co-vary. In the most likely case where X_d=0 (the deuterium excess of water vapor is the same during and outside the rain event as evaporative processes are poorly involved in our study, see section 5-2) and X_D<0 (water vapor isotopic composition is lower during rain event), the ε_D and ε_d trajectories towards negative ΔD_{p_eq} and Δd_{p_eq} as X_D decreases could explain part of the co-variation between ΔD_{p_eq} and Δd_{p_eq} at Plataforma. Indeed, the trajectory of ε_D and ε_d in the $\Delta d_{p\_eq}/\Delta D_{p\_eq}$ diagram follows a constant slope of about 0.07 (the first member in Equation (20)), similar to the slope of the linear regression for Plataforma observations (0.09). However, this cannot explain the most negative disequilibriums. It is worth noting that the co-variation of errors could also play a role at Huaji for the few cases where both disequilibriums are positive (X_D>0, Figure 6).

(2) Considering the most likely case of X_d=0‰ and X_D<0, the upper bounds for the errors are -14.65‰ and -1.02‰ for ΔD_{p_eq} and Δd_{p_eq} respectively.

5-2 Below-cloud rain evaporation and diffusive exchanges

In order to explore the influence of below-cloud evaporation and diffusion processes on the isotopic disequilibriums, we first excluded observations exhibiting an average relative humidity of 100% (17 cases at Huaji) and/or a higher (lower) δD_p (d_p) than δD_{p_target} (d_{p_target}) (9 cases at Huaji). We did not consider either observations for which Δd_{p_eq} or h is not available (17 cases mainly at Plataforma). We therefore examined the 27 remaining cases (9 at Huaji, 18 at Plataforma) following the methodology described in section 3-2. A similar figure to Figure 2 is produced for each of the 27 cases and if Equation (11) applies a value of f is determined. Below-cloud evaporative and diffusive exchanges can be involved in only four cases at Huaji (October 25th, 29th, 30th and April 9th) (see for example Figure 2 done for October 29th and Table 2). The associated evaporative rates vary from 2 to 20% (f from 0.80 to 0.98) pointing out that diffusive exchanges dominate relatively to evaporation (Table 2). The limited influence of evaporation and diffusive exchanges is somewhat surprising. This result must be considered with caution as it may arise from the difference in temporal resolution between water vapor and rain samplings (see section 5-1).

Our result deserves that evaporative effects are responsible for the mostly negative d_p-d_v signal (evaporation decreases d_p and tends to increase d_v as evaporation proceeds) and other processes should explain higher deuterium excess in the surface water vapor phase.

For cases exhibiting a relative humidity of 100% at Huaji, in the common case of a raindrops falling in a richer environment, diffusive exchanges will enrich precipitation (δD_p tends to δD_{p_eq} with $\Delta D_{p\_eq} \leq 0$) and deplete water vapor around it. The efficiency of diffusive exchanges in conditions of saturation could explain the lower negative disequilibriums at Huaji than at Plataforma. However, equilibrium state does not strictly prevail in conditions of surface saturation at Huaji and disequilibrium values for such conditions are comparable to those calculated for lower relative humidity at the same site. We cannot exclude that relative humidity in upper atmospheric levels is lower than at the surface. Other processes could also offset the efficiency of diffusive exchanges as describe in following sections.

5-3 Evapotranspiration from the continental surface

At the first order, plants do not fractionate relative to the water taken up by the roots. They just re-inject the isotopic signal of former precipitation by transpiration in the lower atmosphere. Fast and intense recycling of this vapor, in particular in regions with numerous

679 rainfall events and therefore a permanent relaxation of δD_v to the isotopic composition of
680 former rainfall events, should lead to a small negative isotopic disequilibrium. Indeed,
681 recycling tends to increase δD_v and so δD_{p_eq} is even more difficult to attain (the distance
682 between δD_{p0}, isotopic composition of rain in equilibrium with cloud water vapor, and δD_{p_eq}
683 is increased). This process could explain the small negative ΔD_{p_eq} at Huaji where vegetation
684 is abundant.

685 Evaporation of surface water (soil water or stagnant water) may generate a very
686 depleted flux toward the low-level atmosphere (Craig and Gordon, 1965; Penchenat et al.,
687 2020). For example, using the mean conditions at Huaji for temperature, relative humidity an
688 isotopic composition of water vapor, and considering that the water surface has the isotopic
689 composition of the mean precipitation over the studied period, leads to an isotopic
690 composition of the evaporative flux of ~ -450‰. This induces a depletion of the isotopic
691 composition of near-surface water vapor so that the isotopic composition of precipitation in
692 isotopic equilibrium with this depleted vapor could be lower than δD_p (Penchenat et al.,
693 2020). This evaporative process is actually the only one that could explain the few calculated
694 positive ΔD_{p_eq} (enrichment of precipitation from its expected value at equilibrium),
695 consistently with the correlation between positive ΔD_{p_eq} and the highest values for δD_p in our
696 observations. This process could be at play on the Huaji site (recording 74% of positive
697 ΔD_{p_eq}) where the Zongo stream flows. Unfortunately, it would be very speculative to
698 quantify this process on that site as we actually do not know the isotopic composition of
699 surface water and its possible variation in time.

700 In this section, we do not discuss the impact of transpiration by vegetation and
701 evaporation of surface waters on Δd_{p_eq}. Indeed, the variations of Δd_{p_eq} strongly depend on
702 the isotopic composition of the advected moisture flux and the transpired or evaporated
703 moisture flux as well as on their relative contribution for which we have no information.

704 *5-4 Condensation height*

705 A negative ΔD_{p_eq} may also arise from a high altitude of condensation, above the
706 melting layer. In this case, the initial raindrop is very depleted and it always exhibits lower
707 isotope content than the value that corresponds to isotopic equilibrium with the environment.
708 If exchanges between droplets and water vapor are reduced, the distance to equilibrium will
709 be as large as the altitude of condensation is high. The significant positive relationship

between negative ΔD_{p_eq} and δD_p supports this explanation for negative ΔD_{p_eq}.

5-5 Droplet and rain types

A raindrop falls through an environment more and more enriched relative to the vapor it was formed from. ΔD_{p_eq} will be as negative as the equilibration between the droplets and the surrounding vapor is ineffective. Therefore, a first factor we have to take into account is how much a certain raindrop is exposed to its environment. We assume that small raindrops with low falling velocities come to a more complete equilibrium with surrounding water vapor than big and fast falling raindrops produced by intense rain events (small and slow raindrops offer a larger interactive surface and a smaller terminal velocity (Houze, 1997, 2014; Lee and Fung, 2008). This assumption is hardly addressable from our observations and has already been challenged by some observations in tropical India (Lekshmy et al., 2018). We thus limit the discussion to a few elements.

Our observations mostly capture low precipitation rates favoring the equilibration. This could explain the low disequilibriums in our study and the very significant covariance between δD_p and δD_{p_eq}, suggesting an averaged isotopic equilibrium over the period of observations, although individual coupled rain and water show deviations from equilibrium.

Although there is no relationship between ΔD_{p_eq} and precipitation rate, we found the lowest values of ΔD_{p_eq} (<-30‰, 9 values) among the lowest precipitation rates (<4.1 mm/h). These lowest ΔD_{p_eq} are associated with highly depleted precipitation (Figure 5c). According to several recent studies (Aggarwal et al., 2016; Tharammal et al., 2017; Zwart et al., 2018; Konecky et al., 2019; Sanchez-Murillo et al., 2019), δD_p depletion in tropical rain could be attributed to a large proportion of stratiform rain. In such rain type, hydrometeors grow by vapor diffusion above the melting layer where moisture is relatively depleted in heavy isotopes. Such rain type is supposed to favor isotopic equilibration (low precipitation rate and small raindrop compared to convective rain rains according to Schumacher and Houze et al. (2003)). In case stratiform rain are dominant during our campaigns, our observations suggest that, because of very depleted initial rain, the distance to equilibrium state with low-level water vapor is such large that ΔD_{p_eq} stays mostly negative despite ideal conditions for diffusive exchanges between both water phases. Such negative disequilibriums for dominant stratiform fraction rains have already been observed by Desphande et al. (2010), Lekshmy et al. (2018) and Penchenat et al. (2020). It is worth noting that the complex orography of the

Zongo valley prevents us for examining in details the relationship between ΔD_{p_eq} and the partition between convective to stratiform rain as done in some previous studies (Lekshmy et al., 2018, for example). The use of the usual TRMM (Tropical Rainfall Measuring Mission) product to document this partition in the Zongo region would require a thorough analysis of the radar signal associated with different cloud types in this complex terrain, which requires a dedicated and significant effort beyond the scope of our study (Iguchi et al., 2009).

6- To what extent do local processes influence δ_p and d_p?

Small ΔD_{p_eq} and parallel changes of δD_v and δD_p at both sites suggest that at first order δD_p variations reflect those of the low-level vapor and that local processes are not strong enough to offset the effect of large-scale processes on δD_p. Following the decomposition method explained in section 3-3, we quantify the relative contributions of local and remote processes on δD_p. Large-scale processes explain 79% and 77% of δD_p variability at Huaji and Plataforma respectively (Figure 7a). No significant difference can be seen when differentiating the onset (2005) and the termination (2006) of the rainy season (not shown).

In contrast, the lack of correlation between d_v and d_p, combined with a significant correlation between d_p and of d_p-d_v, suggests that variations of d_p do not reflects those in the low-level vapor and that local effects strongly affect this second order parameter. The Risi et al.'s decomposition shows that local processes explain 75% and 89% of d_p variability at Huaji and Plataforma respectively (Figure 7b). If we separate the onset and the termination of the rainy season for Huaji (no enough data at Plataforma in 2005), we observe that local processes are much stronger at the onset of the wet season (81%, n=14) than at the end of the rainy season (61%, n=21).

A direct conclusion of this section is that δD_p is mainly controlled by large-scale processes, reflecting δD_v, and that post-condensation processes involved as rain falls are poor factors to explain δD_p. This is in agreement with previous work from Vimeux et al. (2011), only based on δD_p observations, which showed that δD_p offers a spatial homogeneity along the Zongo valley despite different precipitation and different in situ post-condensation processes along the valley. This is also consistent with Vuille and Werner (2005), showing that δD_p in the Andes mainly depends on atmospheric processes upstream the site of collection. In contrast, our analysis suggests that local processes have a stronger influence on d_p, offsetting the possibility to explore large-scale signal and moisture source trajectories from

d_p. The influence of local processes on d_p was also suggested by Guy et al. (2019) by comparing d_p series on different stations in the Bolivian and Peruvian Andes, although no quantification of local influence on d_p were done.

7- Conclusions

In this paper, we explore whether the isotopic equilibrium state between water vapor and precipitation prevailed during the onset and the termination of the 2005-2006 wet season in the Bolivian Andes.

Rain and water vapor are very close to the isotopic equilibrium over the whole period of our observations (covariance between δD_p and δD_{p_eq} is of 0.86) although for individual rain events we observed deviations from the equilibration. The distance from isotopic equilibrium is mostly small and negative but deviations can occur for some rain events (20% of disequilibriums have an absolute value higher than 20‰). The Stewart's theory, treating in a uniform manner both evaporative effects and diffusive exchanges, failed to explain major part (~85%) of our observations. Partial evaporation of falling precipitation, one of the key processes controlling tropical and subtropical tropospheric humidity (Folkins and Martin, 2005) is thus, at our sites and during the sampling periods, a very secondary factor in controlling the isotopic composition of both water vapor and precipitation. This result in the Bolivian Andes is consistent with some observations in Sahel (Risi et al., 2008) and in India (Lekshmy et al., 2018). Therefore, other processes or rain characterictics are strong enough to offset below-cloud effects. The height of condensation or the type of rain can explain the negative disequilibriums. Our observations also suggest that significant inputs of evapotranspired moisture at ground level could explain some departures from the isotopic equilibrium. This influence of surface water vapor fluxes has already been suggested by previous studies (Desphande et al., 2010; Lekshmy et al., 2018). Our observations also confirm modeling studies done by Lee and Fung (2008) who simulated a high degree of rain-vapor equilibration in tropical regions on longer timescale than indivudual rain events (above 70% (90%) for deep convective precipitation (stratiform precipitation)).

We also show that the isotopic composition of precipitation and near-surface water vapor closely co-vary: at first order, δ_p is a correct tracer of δ_v and so a correct candidate to reconstruct past large-scale atmospheric processes. In opposite, deuterium excess in precipitation is more affected by local post-condensation processes than isotopes ratio making

this tracer difficult to use to study moisture sources for example.

Our study will need to be completed and confirmed by continuous isotopic measurements in water vapor along a complete rainy season, from November to March, to capture δD_v and δD_p on the same duration. Indeed, the difference in time sampling for rain and water vapor can induce errors on ΔD_{p_eq} and Δd_{p_eq} if the isotopic composition of water vapor largely changes during the rain event. Continuous observations over a complete season will also enable us to have more rain events and to further discuss the isotopic equilibrium on contrasted time scales (individual, sub-seasonal and seasonal scales) as well as the role of rain type (convective versus stratiform) on the equilibration. This is now possible with WS-CRDS laser technology providing continuous isotopic measurements in the water vapor phase (Lee et al., 2006; Gupta et al., 2009; Wen et al., 2010; Tremoy et al., 2011 for some examples).

Acknowledgements

We deeply thank Olivier Cattani, Sonia Falourd and Robert Gallaire for their help for the on-site water vapor collection during the field campaigns; the observers of the COBEE (Compañia Boliviana de Energía Eléctrica) for sampling the event-based precipitation in the Zongo valley in 2005 and 2006 as well as Bénédicte Minster for mass spectrometer analyses at LSCE. We also thank two anonymous reviewers for their very fruitful comments that improved the manuscript as well as Hélène Brogniez, Clémentine Junquas, and Rémy Roca for discussion. This study was funded by the Institut de Recherche pour le Développement (IRD).

References

Aggarwal P.K., Romatschke U., Araguas-Araguas L., Belachew D., Longstaffe F.J., Berg P., Schumacher C., Funk A. (2016) Proportions of convective and stratiform precipitation revealed in water isotope ratios, *Nat. Geosci.* **9**, 624-629.

Aemisegger F., Spiegel J.K., Pfahl S., Sodemann H., Eugeter W., Wernli H. (2015) Isotope meteorology of cold front passages: A case study combining observations and modeling, *Geophys. Res. Lett.* **42**, 5652-5660.

833 Anderson W.T., Bernasconi S.M., McKenzie J.A., Saurer M., Schweingruger F. (2002) Model
834 evaluation for reconstructing the oxygen isotopic composition in precipitation from tree ring
835 cellulose over the last century, *Chem. Geol.* **182**, 121-137.

836 Andrade M., Zaratti F., Forno R., Gutiérrez R., Moreno I., Velarde F., Avila F., Roca M.,
837 Sanchez M-F., Laj P., Jaffrezo J-L., Ginot P., Sellegri K., Ramonet M., Laurent O., Weinhold
838 K., Wiedensohler A., Krejci R., Bonasoni P., Cristofanelli P., Whiteman D., Vimeux F.,
839 Dommergue A., Magand O. (2015) Set to work of a new climate monitoring station in the
840 central andes of Bolivia: the Gaw/Chacaltaya station, *Revista Boliviana de Fisica* **26**, 6-15.

841 Angert A., Lee J.-E., Yakir D. (2008) Seasonal variations in the isotopic composition of near-
842 surface water vapour in the eastern Mediterranean, *Tellus* **60B**, 674-684.

843 Bailey A., Toohey D., Noone D. (2013), Characterizing moisture exchenge between the
844 Hawaiian convective boundary layer and free troposphere using stable isotopes in water, J.
845 *Geophys. Res. Atmos.* **118**, 8208-8221, doi:10.1002/jgrd.50639.

846 Bony S., Risi C., Vimeux F. (2008) Influence of convective processes on the isotopic
847 composition ($\delta^{18}O$ and δD) of precipitation and water vapor in the tropics: 1. Radiative-
848 Convective equilibrium and Tropical Ocean-Global Atmopshere- Coupled Ocean-Atmosphere
849 Response Experiment (TOGA-COARE) simulations, *J. Geophys. Res.* **113***, D19305,*
850 doi:10.1029/2008JD009942.

851 Craig H., Gordon L.I. (1965) Deuterium and oxygen-18 variations in the ocean and the
852 marine atmosphere. *In* E Tongiorgi, ed, Proceedings of a Conference on Stable Isotopes in
853 Oceanographic Studies and Paleotemperatures. Spoleto, Italy, pp 9–130.

854 Dansgaard, W. (1964) Stable isotopes in precipitation, *Tellus* **16***,* 436-468.

855 Deshpande R.D., Maurya A.S., Kumar B., Sarkar A., Gupta K. (2010) Rain-vapor intercation
856 and vapor source identification using stable isotopes from semiarid western India, *J. Geophys.*
857 *Res.* **115***, D23311,* doi:10.1029/2010JD014458.

858 Draxler R.R. and Rolph G.D. (2010) HYSPLIT (HYbrid Single-Particle Lagrangian
859 Integrated Trajectory) Model access via NOAA ARL READY Website
860 (http://ready.arl.noaa.gov/HYSPLIT.php). NOAA Air Resources Laboratory, Silver Spring,
861 MD.

862 Folkins I. and Martin V. (2005) The vertical structure of tropical convection and its impact on
863 the budgets of water vapor and ozone, *J. Atm. Sciences* **62**, 1560-1573.

864 Galewsky J., Steen-Larsen H.C., Field R.D., Worden J., Risi C., Schneider M. (2016) Stable
865 isotopes in atmopsheric water vapo and applications to the hydrologic cycle, *Rev. Geophys.*
866 **54**, 809-865, doi:10.1002/2015RG000512.

867 Graf P., Wernli H., Pfahl S., Sodemann H. (2019) A new interpretative framework for below-
868 cloud effects on stable isotopes in vapour and rain, *Atmos. Chem. Phys.* **19**, 747-765.

869 Guilpart E., Vimeux F., Evan S., Brioude J., Metzger J.-M., Barthe C., Risi C., Cattani O.
870 (2017) The isotopic composition of near-surface water vapor at tje Maïdo observatory
871 (Reunion Island, southwestern Indian Ocean) documents the controls of the humidity of the
872 subtropical troposphere, *J. Geophys. Res.* **122**, 9628-9650, doi:10.1002/2017JD026791.

873 Gupta, P., Noone D., Galewsky J., Sweeney C., Vaughn B.H. (2009) Demonstration of high-
874 precision continuous measurements of water vapor isotopologues in laboratory and remote
875 field deployment using wavelenght-scanned cavity ring-down spectroscopy (WS-CRDS)
876 technology, *Rapid Commun. Mass Spectr.* **23**, 2534–2542.

877 Guy H., Seimon A., Perry L.B., Konecky B.L., Rado M., Andrade M., Potocki M., Mayewski
878 P.A. (2019) Subseasonal variations of stable isotopes in Tropical Andean precipitation, *J.*
879 *Hydrometeor.* (2019) **20**, 915–933.

880 Jouzel J., Merlivat L. (1984) Deuterium and oxygen 18 in precipitation: Modeling of the
881 isotopic effects during snow formation, *J. Geophys. Res.* **89***,* 11749-11757.

882 Houze R.A. (1997) Stratiform precipitation in regions of convection: A meteorological
883 paradox?, *Bull. Amer. Met. Soc.* **78**, 2179-2196.

884 Houze R.A. (2014) Clouds Dynamics, International Geophysics Series vol. 104, Academic
885 Press, ISBN 9780123742667.

886 Iguchi, T., T. Kozu, J. Kwiatkwoski, R. Meneghini, J. Awaka, and K. Okamoto (2009)
887 Uncertainties in the Rain Profiling Algorithm for the TRMM Precipitation Radar, *J. Meteor.*
888 *Soc. Japan* **87A**, 1-30.

889 Junquas C., Takahashi K., Condom T., Espinoza J.-C., Chavez S., Sicart J.-E., Lebel T.,
890 (2018) Understanding the influence of orography on the precipitation diurnal cycle and the

associated atmospheric processes in the central Andes, *Clim. Dyn.* **50**, 3995-4017.

Konecky B.L., Noone D.C., Cobb K.M. (2019) The influence of competing hydroclimate processes on stable isotope ratios in tropical rainfall, *Geophys. Res. Lett.* **46**, 1622-1633.

Kurita N. (2013) Water isotopic variability in response to mesoscale convective system over the tropical ocean, *J. Geophys. Res.* **118***,* 10376-10390.

Laskar A.H., Huang Jr-C., Hsu S-C., Bhattacharya S. K., Wang, C-H., Liang M-C. (2014) Stable isotopic composition of near surface atmospheric water vapor and rain-vapo interaction in Taipei, Taiwan, *J. Hydrol.* **519**, 2091-2100.

Lee X., Smith R., Williams J. (2006) Water vapour $^{18}O/^{16}O$ isotope ratios in surface air in New England, USA, Tellus B 58, 293-304.

Lee J.-E., Fung I. (2008) Amount effect of water isotopes and quantitative analysis of post-condensation processes, *Hydrological processes* **22**, 1, 1-8.

Lekshmy P.R., Midhun M., Ramesh R. (2018) Influence os stratiform clouds on δD and $\delta^{18}O$ of monsoon water vapour and rain at two tropical coastal stations*, J. Hydrol.* **563**, 354-362.

Majoube M. (1971) Fractionnement en oxygène 18 et en deuterium entre l'eau et la vapeur, *Journal de Chimie et de Physique* **68**, 1423-1436.

Managave S. R., Jani R. A., Rao T. N., Sunilkumar K., Satheeshkumar S., Ramesh, R. (2016) Intra-event isotope and raindrop size data of tropical rain reveal effects concealed by event averaged data, *Clim. Dyn.* **47**, 981–987.

Marengo J.A., Soares W.R., Saulo C., Nicolini M. (2004) Climatology of the low level jet east of the Andes as derived from the NCEP-NCAR reanalysis. Characteristics and temporal variability, *J. Clim* **17**, 2261-2280.

Merlivat L. (1978) Molecular diffusivities of $H_2{}^{16}O$, $HD^{16}O$ and $H_2{}^{18}O$ in gases, *J. Chem. Phys.* **69**, 2864-2871.

Penchenat T., Vimeux F., Daux V., Cattani O., Viale M., Villalba R., Srur A., Outrequin C. (2020) Isotopic equilibrium between precipitation and water vapor in Northern Patagonia and its consequences on $\delta^{18}O$cellulose estimate, *J. Geophys. Res.,* **125**, e2019JG005418.

Risi C., Bony S., Vimeux F. (2008) Influence of convective processes on the isotopic composition of precipitation and water vapor in the tropics: 2. Physical interpretation of the amount effect, *J. Geophys. Res.* **113**, D19306, doi:10.1029/2008JD009943.

Risi C., Bony S., Vimeux F., Frankenberg C., Noone D., Worden J. (2010) Understanding the Sahelian water budget through the isotopic composition of water vapor and precipitation, Journal of Geophysical Research, *J. Geophys. Res.* **115**, D24110, doi:10.1029/2010JD014690.

Rolph G.D. (2010) Real-time Environmental Applications and Display sYstem (READY) Website (http://ready.arl.noaa.gov). NOAA Air Resources Laboratory, Silver Spring, MD.

Ronchail J. (1989) Advections polaires en Bolivie: mise en évidence et caractérisation des effets climatiques, *Hydrologie continentale* **4**, 49-56.

Sanchez-Murillo R., Duran-Quesada A., Esquivel-Hernandez G., Rojas-Cantillano D., Birkel C., Welsh K., Sanchez-Llull M., Alonso-Hernandez C.M., Tetzlaff D., Soulsby C., Boll J., Kurita N.n Cobb K.M. (2019) Deciphering key processes controlling rainfall isotopic variability during extreme tropical cyclones, *Nature Communications* **10:4321**, doi:10.1038/s41467-019-12062-3.

Schumacher C., Houze R. (2003) Stratiform rain in the Tropics as seen by the TRMM precipitation Radar, *J. Clim.* **16**, 1739-1756.

Sinha N., Chakraborty S. (2020) Isotopic interaction and source moisture control on the isotopic composition of rainfall over the Bay of Bengal, *Atmos. Reas*. **235**, 10.1016/j.atmosres.2019.104760.

Srivastava R., Ramesh R., Gandhi N., Jani R.A., Singh A.K. (2015) Monsoon onset signal in the stable oxygen and hydrogen isotope ratios of monsoon vapor, *Atmos. Env.* **108**, 117-124.

Stewart M.K. (1975) Stable isotope fractionation due to evaporation and isotopic exchange of falling waterdrops: Applications to atmospheric processes and evaporation of lakes, *J. Geophys. Res.* **80**, 1133-1146.

Tharammal T., Bala G., Noone D. (2017) Impact of deep convection on the isotopic amount effect in tropical precipitation, *J. Geophys. Res.* **122**, 1505-1523.

Tremoy G., Vimeux F., Cattani O., Mayaki S., Souley I., Favreau G. (2011) Water vapor isotope ratios measurements with Wavelength-Scanned Cavity Ring-Down Spectroscopy

(WS-CRDS) technology: new insights and important caveats for deuterium excess measurements in tropical areas in comparison with isotope-ratio mass spectrometry (IRMS)**,** *Rapid Commun. Mass Spectrom.* **25**, 3469-3480.

Tremoy G., Vimeux F., Soumana S., Souley I., Risi C., Favreau G., Oï M. (2014) Clustering mesoscale convective systems with laser-based water vapor $\delta^{18}O$ monitoring in Niamey (Niger), *J. Geophys. Res.* **119**, 5079-5013.

Vimeux F., Gallaire R., Bony S., Hoffmann G., Chiang J-C., What are the climate controls on isotopic composition (δD) of precipitation in Zongo Valley (Bolivia) ? (2005) Implications for the Illimani ice core interpretation, *Earth Planet. Sci. Lett.* **240**, 205-220.

Vimeux F., Tremoy G., Risi C., Gallaire R. (2011) A strong control of South American SeeSaw on the intra-seasonal variability of the isotopic composition of precipitation in the Bolivian Andes, *Earth Planet. Sci. Lett.* **307**, 47-58.

Vuille M. and Werner M. (2005) Stable isotopes in precipitation recording South American summer monsoon and ENSO variability: observations and model results, *Clim. Dyn.* **25**, doi:10.1007/s00382-005-0049-9.

Wang S., Zhang M., Che Y., Zhu X., Liu X. (2016) Influence of below-cloud evaporation on deuterium excess in precipitation of arid Central Asia and its meteorological controls, *J. Hydrometeor.* **17**, 1973–1984.

Welp L.R., Lee X., Griffis T.J., Wen X.-F., Xiao W., Li S., Sun X., Hu Z., Val Martin M., Huang J. (2012) A meta-analysis of water vapor deuterium excess in the midlatitude atmospheric surface layer, *Global Biogeochem. Cycles* **26**, GB3021, doi:10.1029/2011GB004246.

Wen X.F., Zhang S.C., Sun X.M, Yu G.R., Lee X. (2010) Water vapor and precipitation isotope ratios in Beijing China, *J. Geophys. Res*. **115***,* D01103, doi: 10.1029/2009JD012535.

Wiedensohler A., Andrade B., Weinhold K., Müller T., Birmilia W., Velarde F., Moreno I., Forno R., Sanchez M.F., Laj P., Ginot P., Whiteman D.N., Krejcif R., Sellegri K., Reichler T. (2018) Black carbon emission and transport mechanisms to the free troposphere at the La Paz/El Alto (Bolivia) metropolitan area based on the Day of Census (2012), *Atmos. Environ*. **194**, 158-169.

Yakir D. and Wang X.F. (1996) Fluxes of CO2 and water between terrestrial vegetation and the atmopshere estimated from isotope measurements, *Nature* **279**, 404-406

Yakir D. and Sternberg da S.L. (2000) The use of stable isotopes to study ecosystem gas exchange, *Oecologia* **123**, 3, 297-311.

Yao T., Zhang X., Guan H., Zhou H., Hua M., Wang X. (2018) Climatic and environmental controls on stable isotopes in atmopsheric water vapor near the surface observed in Changsha, China, *Atmos. Env.* **189**, 252-263.

Zwart C., Munksgaard N.C., Protat A., Kurita N., Lambrinidis D., Bird M. (2018) The isotopic signature of monsoon, cloud modes, and rainfall type, *Hydrological Processes* **32**, 2296-2303.

Figure captions

Figure 1: (a) Cross-section of the Zongo valley in the Northeast-Southwest direction with the sites of Huaji (945 m), Plataforma (4750 m) and Chacaltaya observatory (5240 m) (black rectangles). The main moisture flow along the Andean slope from the Amazon basin, associated to the South American Low Level Jet (SALLJ), is mentioned by the red arrows and (b) Google Earth map of the Zongo Valley with the location of Huaji (945 m) and Plataforma (4750 m) as well as the five pluviometers located at Harca (1480 m), Sainani (2210 m), Botijlaca (3492 m), Tiquimani (3900 m) and Zongo (4264 m) sites. The location of Chacaltaya observatory is also indicated. Red arrows represent the channelization of moisture flux inside the valley. Google Earth image (5 May 2020). Bolivia. Images CNES/Airbus, Maxar Technologies, Eye alt. 61 km, US Department of State Geographer (https://earth.google.com/web/).

Figure 2: Diagram showing Δd_{p_eq} as a function of ΔD_{p_eq} for October 29th, 2005 at Huaji (T=24 °C, h=87.3%). Orange line is the theoretical trajectory of initial droplet P_0 as z (altitude of the droplet formation in the cloud at isotopic equilibrium with water vapor) varies from 0 to 3 km at T=24 °C. The isotopic composition of the initial cloud water vapor (δD_{v0} and d_{v0}) is obtained from the observed δD_v and d_v by applying the isotopic altitudinal gradients calculated in section 4-5 for z varying from 0 to 3 km. The isotopic composition of the initial precipitation P_0 (δD_{p0} and dp_0) is then calculated at equilibrium with cloud water vapor considering a lapse rate of -5.1°C/km (Vimeux et al., 2011). The orange circle is P_0 for z=3 km. The theoretical isotopic equilibrium is plotted on (0,0) (P_{eq}, light blue circle) and P_0 is equal to P_{eq} for z=0 km. Green line is the theoretical trajectory of P_{target} (f=0) as h decreases from 100% (P_{target} = P_{eq}) at T=24 °C. The green circle is P_{target} for h=87.3%. Purple line is the trajectory of precipitation for h=87.3% and T=24 °C as f varies from 1 (P_0) to 0 (P_{target}). The intercept between the orange and purple theoretical curves is obtained for f=1 and it determines P_0 (red circle) at z=0.6 km for this specific day. The observations (P_{obs}, blue square) can be explained by the Stewart's theory and corresponds to f=0.98 (f^{β} can be calculated or graphically deduced as the ratio between the distance between P_{obs} and P_{target} and the distance between P_0 and P_{target}). In the general case, when no intercept is found between the trajectory of precipitation (purple line) and the trajectory of initial precipitation (orange line), the Stewart's theory does not apply.

Figure 3: Comparison of precipitation (in mm) over the 2005-2006 (light green) rainy season

with the mean 2000-2011 rainy season (dark green) in the Zongo valley for (a) 5 stations in the Zongo valley (Harca, Sainami, Botijlaca, Tiquimani and Zongo) (precipitation for one station is the sum of precipitation from October to April); (b) each month from October to April (precipitation for one month is the sum of precipitation over the 5 stations).

Figure 4: Isotopic composition (δD, ‰ V-SMOW) and deuterium excess (d, ‰ V-SMOW) in precipitation (stars) and water vapor (circle) at Huaji (red), (blue) and Layca Cota (green) during the 2005 and 2006 field campaigns. When several precipitation events occur within a day, the daily amount-weighted isotopic composition is calculated and shown here. The date for water vapor data corresponds to the day where the vapor sample is collected. When available in both phases, the difference of deuterium excess between rain and water vapor is also shown (squares).

Figure 5: Distribution of ΔD_{p_eq} (‰) (a) at Plataforma and Huaji and (b) in 2005 and 2006; (c) ΔD_{p_eq} (‰) as a function of δD_p (‰) for the whole 2005-2006 time period.

Figure 6: Δd_{p_eq} (‰) as a function of ΔD_{p_eq} (‰) for the 54 simultaneous deuterium and deuterium excess disequilibriums (Huaji 2005: red circles, Huaji 2006: green circles, Plataforma 2005: blue circles and Plataforma 2006: black circles). We also show how ε_d (‰) varies as a function of ε_D (‰) for different values of X_D (from -15 to 10‰), and for three values of X_d (X_d=0‰ red arrows, X_d=0.5‰ orange arrows, X_d=2‰ dark yellow arrows).

Figure 7: (a) Decomposition of δD_p into a large-scale signal (associated to δD_v, square) and a local effect (associated to δD_p-δD_v, circle) for Huaji (red) and Plataforma (bleck). Those contributions are plotted as a function of δD_p for the whole dataset following the decomposition of Risi et al., (2010); (b) same as (a) but for deuterium excess.

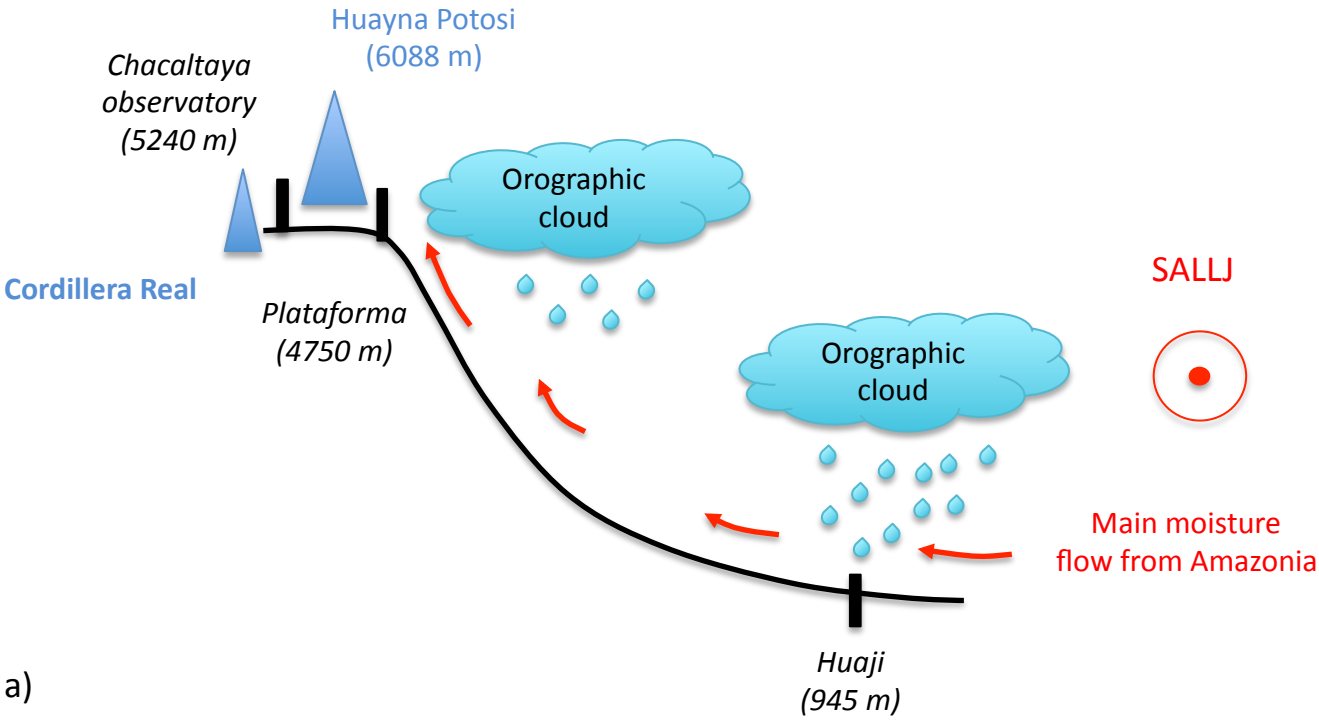
Huayna Potosi
(6088 m)
Chacaltaya
observatory
(5240 m)
Orographic
cloud
Cordillera Real
Plataforma
(4750 m)
SALLJ
Orographic
cloud
Main moisture
flow from Amazonia
Huaji
(945 m)

a)

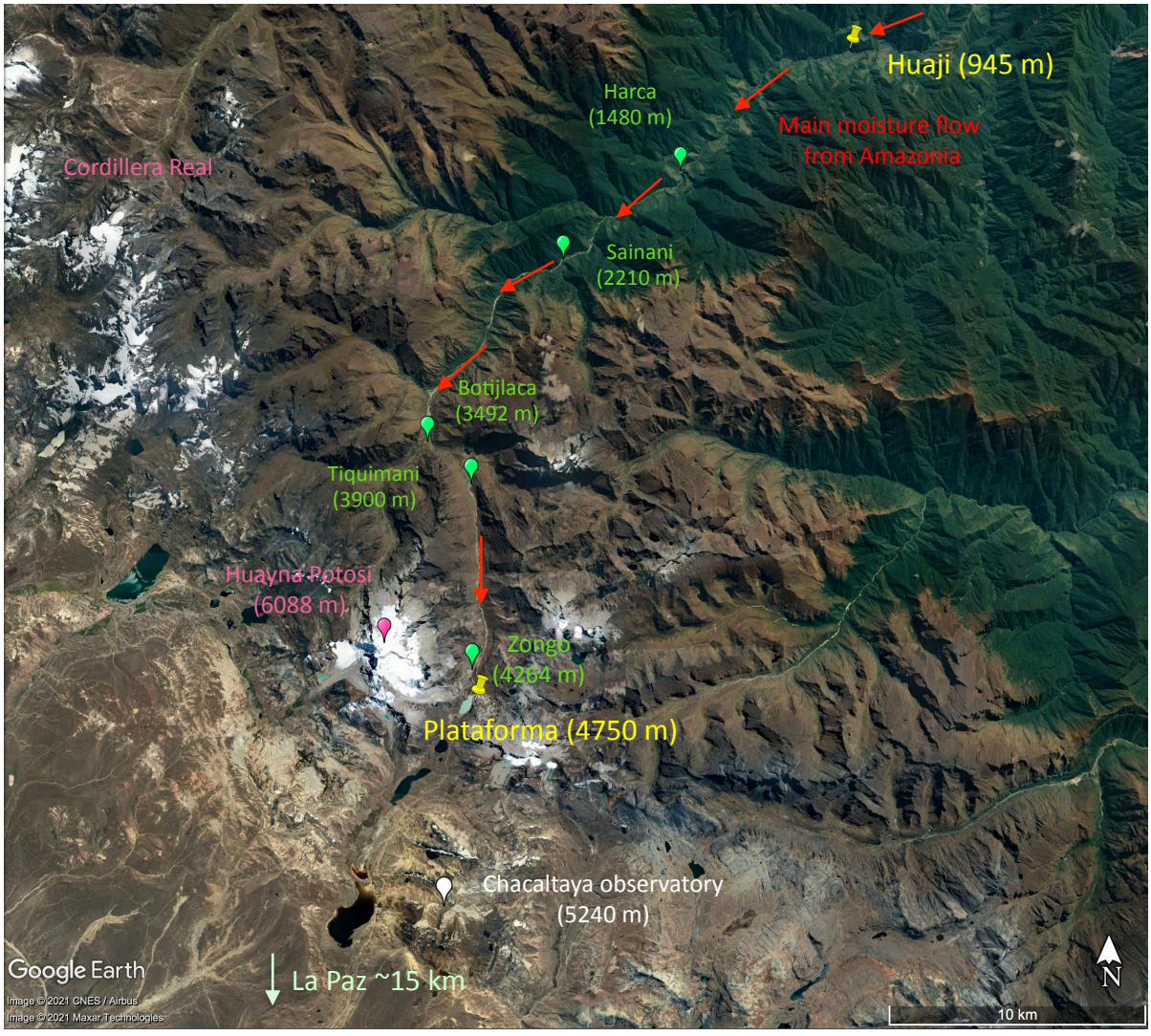
Huaji (945 m)
Harca
(1480 m)
Main moisture flow
from Amazonia
Cordillera Real
Sainani
(2210 m)
Botijlaca
(3492 m)
Tiquimani
(3900 m)
Huayna Potosi
(6088 m)
Zongo
(4264 m)
Plataforma (4750 m)
Chacaltaya observatory
(5240 m)
Google Earth
La Paz ~15 km
N
10 km

b)

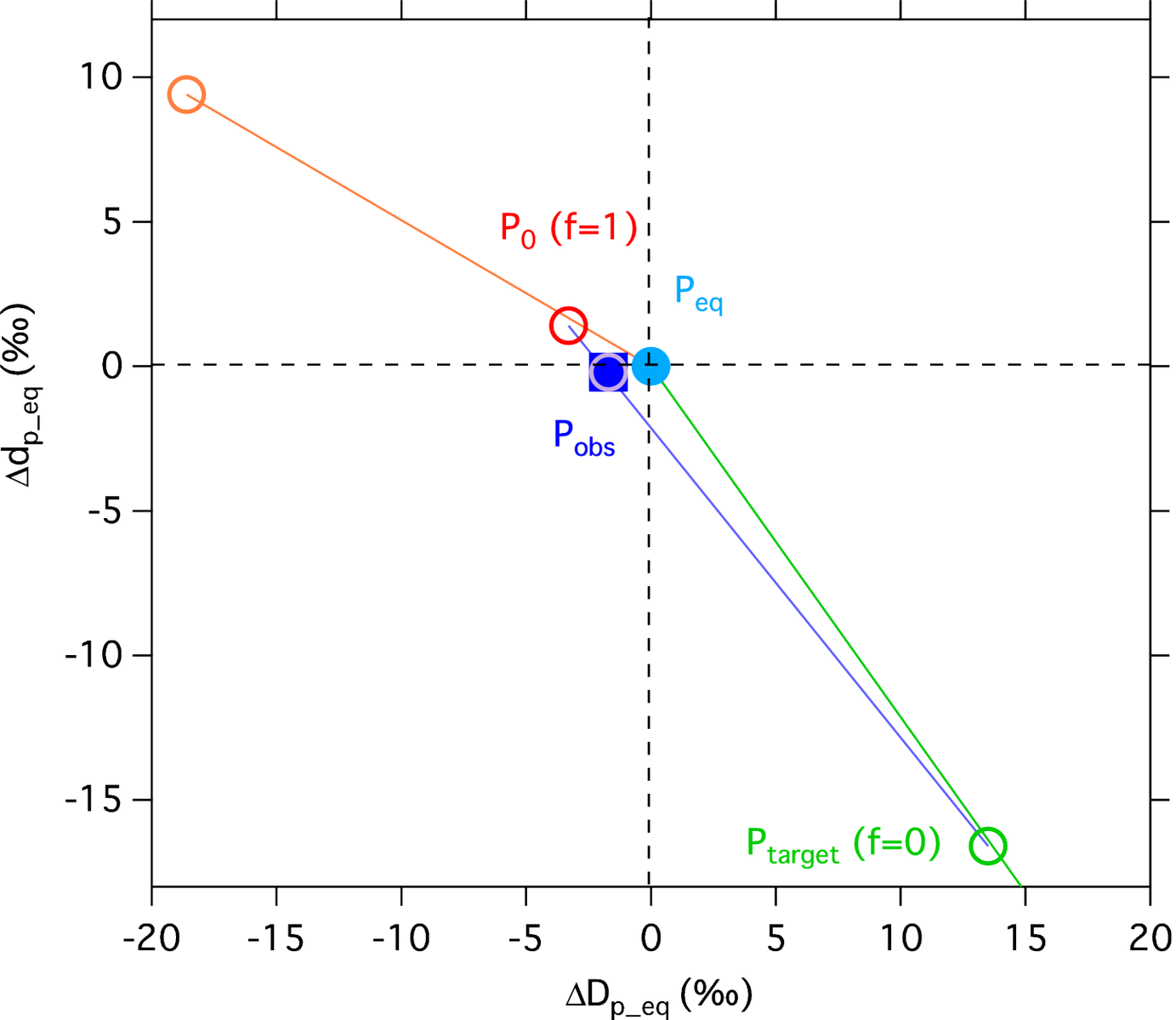

Huaji, October 29th 2005, T=24 °C, h= 87.3% (P_{obs})

Initial precipitation (P_0) for z=0 to 3 km

Initial precipitation (P_0) for z=3 km

Initial precipitation (P_0) for z=0.6 km

Target precipitation for h decreasing from 100%

Target precipitation for h= 87.3% (P_{target})

Target precipitation for h= 100% (P_{eq})

Precipitation for f=1 to 0, h=87.3%, T=24 °C

Precipitation for f= 0.98 (P_{obs})

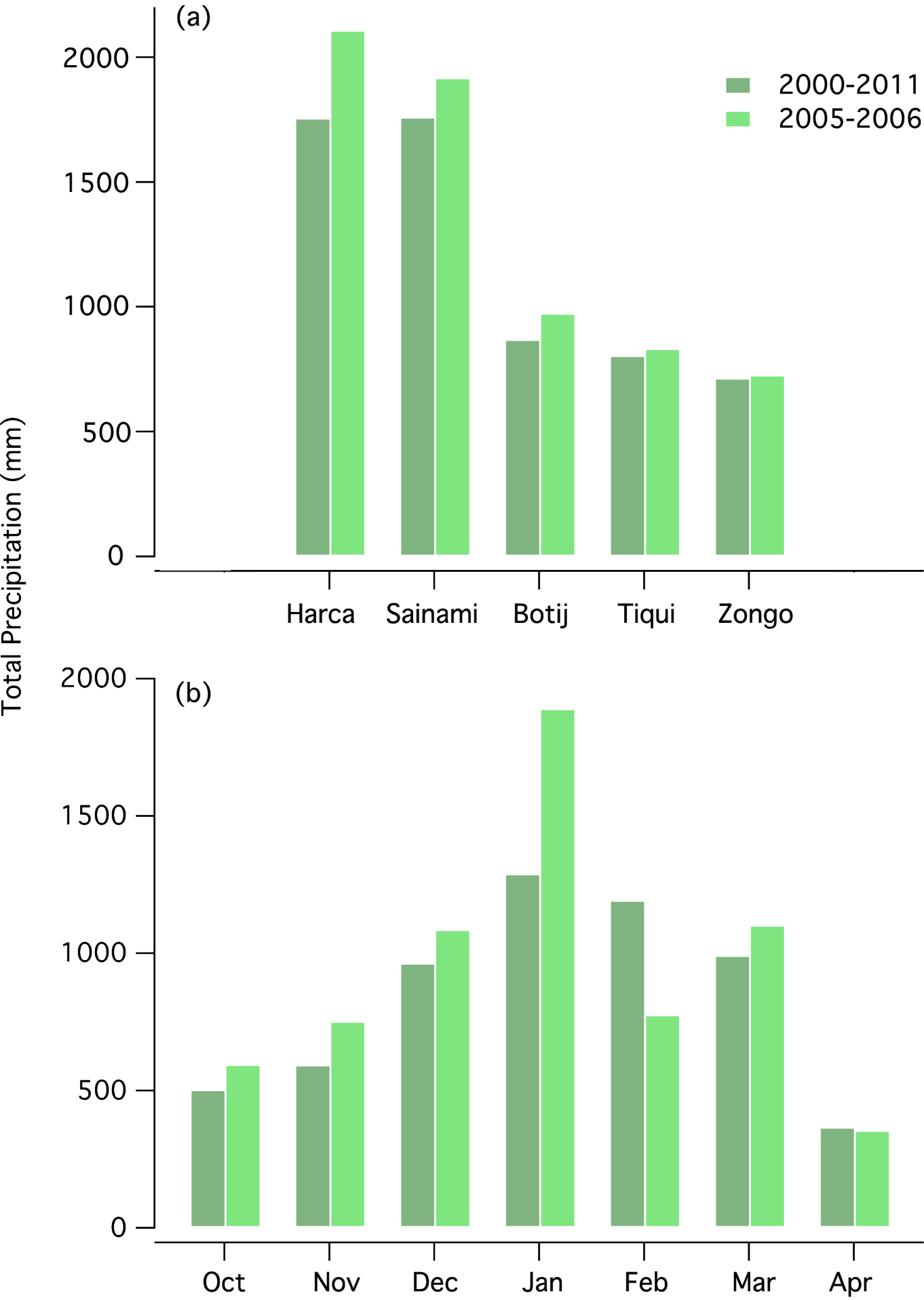
(a)
2000
1500
1000
500
0
2000-2011
2005-2006
Total Precipitation (mm)
Harca
Sainami
Botij
Tiqui
Zongo
(b)
2000
1500
1000
500
0
Oct
Nov
Dec
Jan
Feb
Mar
Apr

Huaji vapor
Huaji precipitation
Plataforma vapor
Plataforma precipitation
Laïca Cota precipitation
Huaji d_p-d_v
Plataforma d_p-d_v

δD (‰)

0
-50
-100
-150
-200
-250

d (‰)

30
25
20
15
10
5
0

d_p-d_v (‰)

10
5
0
-5
-10
-15

25.10.2005
6.11.2005
18.11.2005
18.3.2006
4.4.2006
21.4.2006

Date (dd.mm.yyyy)

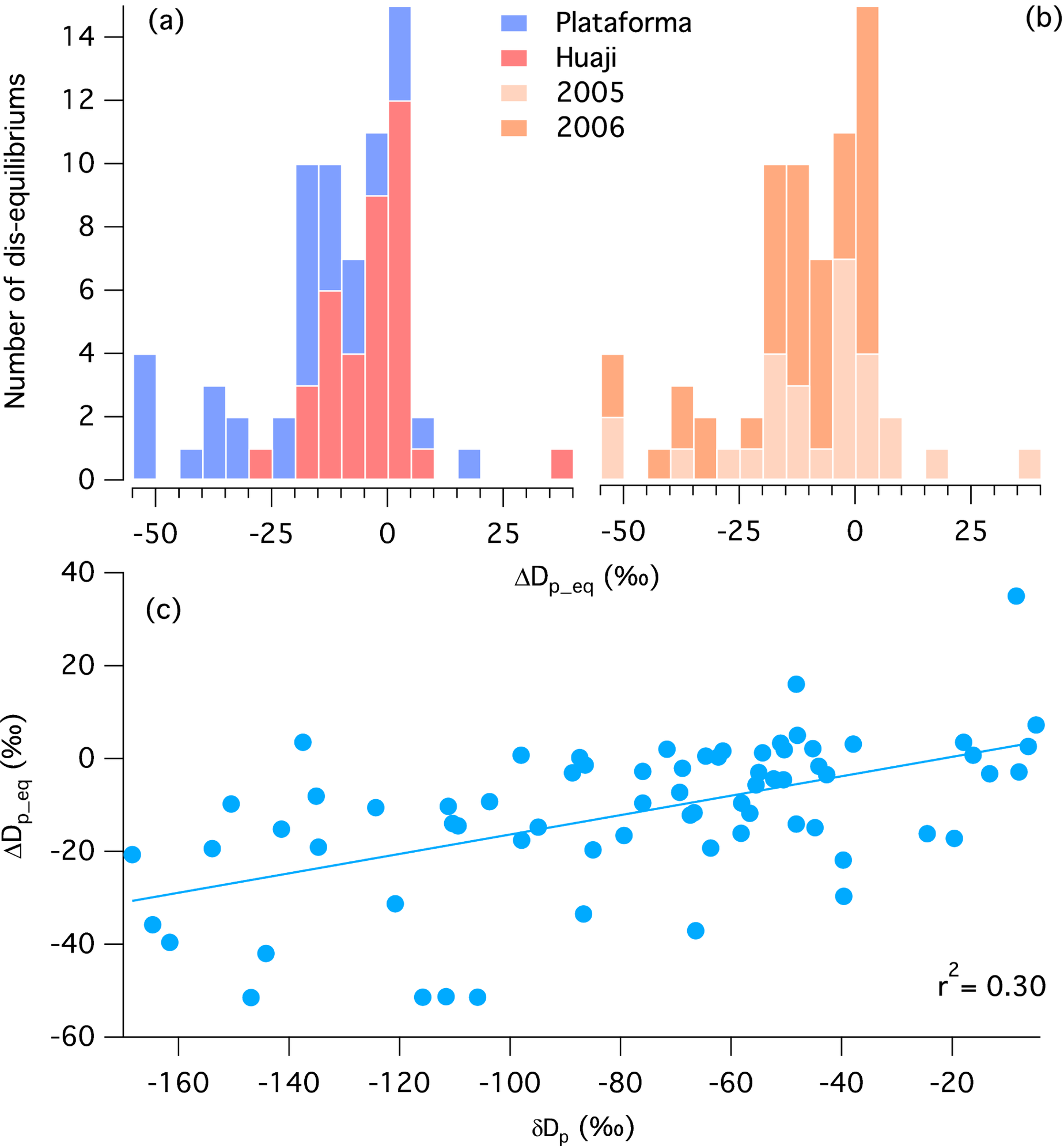
(a)
(b)
(c)
Plataforma
Huaji
2005
2006
Number of dis-equilibriums
0
2
4
6
8
10
12
14
-50
-25
0
25
ΔDp_eq (‰)
40
20
0
-20
-40
-60
-160
-140
-120
-100
-80
-60
-40
-20
δDp (‰)
r2 = 0.30

Huaji 2005
Huaji 2006
Plataforma 2005
Plataforma 2006
Linear regression of Plataforma observations
Trajectory of ε_d as a function of ε_D for X_d=0 ‰ ($\varepsilon_d/\varepsilon_D$=0.07)
Trajectory of ε_d as a function of ε_D for X_d=0.5 ‰
Trajectory of ε_d as a function of ε_D for X_d=2 ‰

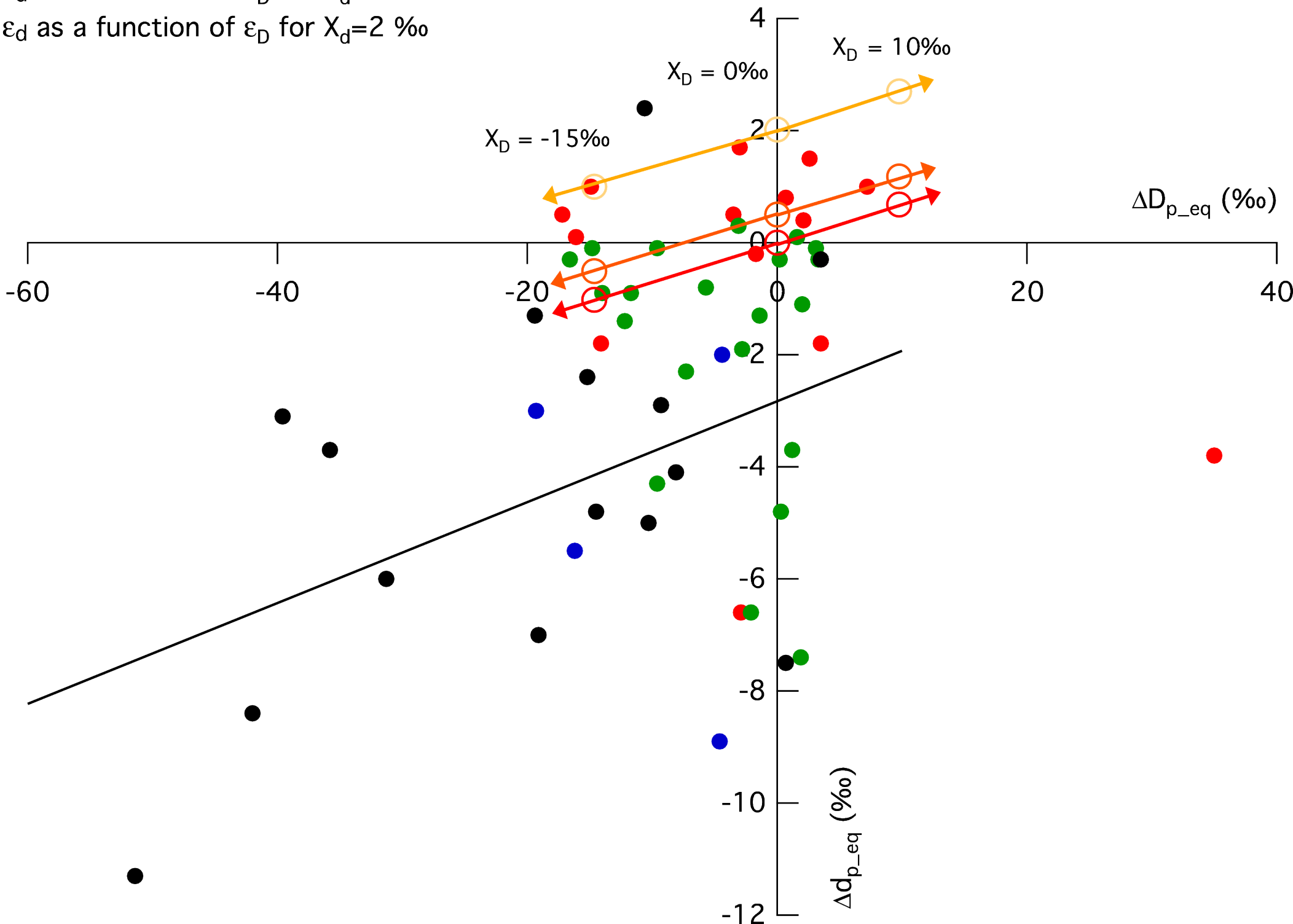

Large-scale effects
Local effects

Huaji δD_v
Huaji δD_v - δD_v
Plataforma δD_v
Plataforma δD_v - δD_v

(a)

y = 0.23x + 94.37
r^2 = 0.30 (p<0.001)

y = 0.21x + 80.71
r^2 = 0.30 (p<0.001)

y = 0.77x - 94.37
r^2 = 0.83 (p<0.001)

y = 0.79x - 80.71
r^2 = 0.87 (p<0.001)

Contribution to δD_p (‰)

150
100
50
0
-50
-100
-150
-200
-250

-150
-100
-50
0

δD_p (‰)

Huaji d_v
Huaji d_p - d_v
Plataforma d_v
Plataforma d_p - d_v

(b)

y = 0.11x + 19.97
r^2 = 0.02 (p<0.1)

y = 0.25x + 12.06
r^2 = 0.17 (p<0.05)

y = 0.75x - 12.06
r^2 = 0.65 (p<0.001)

y = 0.89x - 19.97
r^2 = 0.56 (p<0.001)

Contribution to d_p (‰)

25
20
15
10
5
0
-5
-10
-15

5
10
15
20
25

d_p (‰)

Table 1: mean±1σ for surface relative humidity and temperature and water isotopic composition (δD_v, δD_p, d_v, d_p) and mean[68%-confidence interval] for precipitation rate (it follows a log-normal distribution) during the two field campaigns at Huaji (2005 campaign: October 23th-Nov 21st, 2006 campaign: March 15th-May 1st) and Plataforma (2005 campaign: October 23th-Nov 27th, 2006 campaign: March 11th-April 30th). All rain events occurring within the field campaigns are taken into account for the calculation of δD_p, d_p and precipitation rates. The isotopic composition of precipitation is amount-weighted.

Field campaign	**2005**	**2006**
	m±1σ or m[68%-confidence interval]	m±1σ or m[68%- confidence interval]
Relative humidity (%)		
Huaji	88.1±17.0	92.7±12.3
Plataforma	69.6±22.2	68.1±22.2
Temperature (°C)		
Huaji	22.8±4.6	21.1±4.0
Plataforma	2.3±2.7	2.3±2.5
Precipitation rate (mm/h)		
Huaji	4.7[1.2-7.7]	4.8[1.0-8.7]
Plataforma	1.6[0.8-2.4]	1.4[0.5-2.3]
δD_v (‰)		
Huaji	-98.0±13.7	-136.3±12.3
Plataforma	-141.1±30.3	-181.0±24.6
δD_p (‰)		
Huaji	-40.6±30.2	-79.1±24.1
Plataforma	-82.9±56.5	-124.3±34.7
d_v (‰)		
Huaji	14.9±1.4	14.1±1.8
Plataforma	18.9±4.4	21.1±3.3
d_p (‰)		
Huaji	10.9±3.4	9.7±2.4
Plataforma	17.8±3.3	16.1±2.2

Table 2: Disequilibriums (ΔD_{p_eq}, ‰), temperature (T, °C), precipitation rate (P, mm/h), relative humidity (h, %) and drops evaporated fraction (1-f, %) when ΔD_{p_eq} can be explained by the Stewart's theory. Temperature and relative humidity are averaged over the rain period.

Site and date	**ΔD_{p_eq} (‰)**	**Δd_{p_eq} (‰)**	**T (°C)**	**P (mm/h)**	**h (%)**	**1-f (%)**
Huaji October 25, 2005	-14.9	-1.0	25.5	8.0	83.3	20
Huaji October 29, 2005	-1.7	-0.2	24.0	3.0	87.3	2
Huaji, October 30, 2005	-3.4	0.5	24.0	2.5	88.0	2
Huaji, April 9, 2006	-2.8	-1.9	23.6	-	91.5	6